Exchanges of Atmospheric CO_2 and $^{13}CO_2$ with the Terrestrial Biosphere and Oceans from 1978 to 2000. II. A Three-Dimensional Tracer Inversion Model to Deduce Regional Fluxes

Stephen C. Piper[1], Charles D. Keeling[1], Martin Heimann[2], and Elisabeth F. Stewart[1]

Abstract— **A three-dimensional tracer inversion model is described that couples atmospheric CO_2 transport with prescribed and adjustable source/sink components of the global carbon cycle to predict atmospheric CO_2 concentration and $^{13}C/^{12}C$ isotopic ratio taking account of exchange fluxes of atmospheric CO_2 with the terrestrial biosphere and the oceans. Industrial CO_2 emissions are prescribed from fuel production data. Transport of CO_2 is prescribed by a model, TM2, that employs 9 vertical levels from the earth's surface to 10 mb, a numerical time step of 4 hours, and a grid spacing of approximately 8° of latitude and 10° of longitude. Horizontal advection is specified from analyzed observations of wind. Vertical advection is consistent with mass conservation of wind within each grid box. Convective mixing and vertical diffusion are determined at each time step from meteorological data. The source/sink components represent various CO_2 exchanges, some sources to the atmosphere, others sinks. The study focuses on establishing interannual variability in net terrestrial biospheric and net oceanic fluxes with the atmosphere revealed by variability in atmospheric CO_2, taking account of possible stimulation of land plant growth ("CO_2 fertilization") and oceanic CO_2 uptake, as well as industrial CO_2 emissions. Net primary production of land plants (NPP) and heterotrophic respiration are specified to vary only seasonally, on the basis of data averaged from 1982-1990, inclusive. NPP is determined from a vegetative index, NDVI, derived from remotely sensed radiometric data from satellites. Heterotrophic respiration is a function of surface air temperature. Oceanic exchange of CO_2 varies seasonally as specified by a coefficient of CO_2 gas exchange. Spatial variability of all source/sink components is specified for each 8° x 10° grid box of TM2, *a priori*, for 5 terrestrial biospheric and 5 oceanic source/sink components, and with respect to emissions of industrial CO_2. Spatial variations of terrestrial exchange are made proportional to NPP. Heterotrophic respiration similarly varies by setting its annual average for each grid box equal to NPP. Spatial variations in oceanic CO_2 exchange take account of gas exchange dependence on wind speed and temperature and, in the tropics, on a time-invariant spatially variable specification of the partial pressure of CO_2 of surface sea water, based on direct observations. Carbon-isotopic fractionation is taken into account for all chemical processes modeled. To produce an optimal fit to observations of atmospheric CO_2, the inversion model adjusts the magnitude of 7 additional source/sink components divided with respect to tropical, temperate, and polar geographic zones. There are 4 terrestrial zones, excluding a southern polar zone of negligible importance. There are 3 oceanic zones: one tropical, and one combined temperate/polar zone in each hemisphere. Calculations are carried out in a quasi-stationary mode that repeats a single annual cycle 4 times, and saves the results for the final year. Alternatively, the model has been run in an extended response mode that takes account of a 4-year history of atmospheric CO_2 response to a pulse introduced during the first year of this history. Interannual variations in exchange are established by adjusting the model to predict atmospheric CO_2 concentration and $^{13}C/^{12}C$ ratio averaged for annual periods at overlapping 6-month intervals. Net CO_2 exchange fluxes, seasonally adjusted, were determined from 1981-1999, inclusive, using atmospheric CO_2 data reported by Keeling et al. [2001].**

[1]Scripps Institution of Oceanography, University of California, San Diego, California

[2]Max Planck Institute for Biogeochemistry, Jena, Germany

PREFACE

This is the second of four articles that seeks to characterize sources and sinks of atmospheric carbon dioxide from direct measurements of the concentration and $^{13}C/^{12}C$ ratio of atmospheric CO_2. The articles, organized as though chapters of a single study, are referred to henceforth as Articles I to IV corresponding, respectively, to Keeling et al. [2001], Piper et al. [2001a,b], and Keeling and Piper [2001].

1. INTRODUCTION

If the circulation of the atmosphere and the spatial and temporal variations in CO_2 concentration and $^{13}C/^{12}C$ isotopic ratio are realistically accounted for, it is possible, in principle, to determine the strength of exchanges of atmospheric CO_2 with the land and the oceans. Such an inverse deduction of causes from their effects, is not readily achieved, however. Carried out for an open system involving only part of the globe, it is unreliable because fluxes of CO_2 across atmospheric boundaries are difficult to establish except by resorting to a global-scale fully three-dimensional calculation. Gathering adequate data for such a global calculation, however, is a daunting task.

Presently atmospheric CO_2 data are available to calculate CO_2 gradients from about 140 fixed locations world-wide, supplemented by data from ships and aircraft. Data for CO_2 concentration are more extensive than isotopic data [Masarie and Tans, 1995, and GLOBALVIEW website communication]. Yet even if the number of observing stations were greatly expanded, fine scale east-west resolution of regional sources and sinks would be difficult, because longitudinal gradients, reflective of these fluxes, are barely detectable owing to strong zonal atmospheric mixing. Also, important natural fluxes of CO_2 in mid-northern latitudes can be determined by an inverse calculation only if large industrial CO_2 emissions can be precisely specified in time and space independently. Thus, it is presently possible to establish CO_2 sources and sinks by inversion of atmospheric CO_2 data only on broad spatial scales and with considerable time-averaging.

Over a decade ago, we carried out such a study [Keeling et al., 1989a,b; Heimann et al., 1989]. Since then numerous

additional studies have clarified the value and limitations of such calculations, including a series of articles on the "Breathing of the Earth" in 1996 [Rayner et al.; Monfray et al.; Denning et al., a, b; Bousquet et al.; Jain et al.] and several still more recent studies [e.g., Law et al., 1996; Rayner et al., 1999a,b; Bousquet et al., 1999a,b; Kaminski et al, 1999; Heimann et al., 1998; Heimann and Kaminski, 1999]. Evidently, different models agree closely in their predictions of time-varying sources and sinks only when applied to broad zonal regions [Heimann, 2000].

After addressing global scale carbon fluxes in Article I, we focus here, in Article II, on a regional analysis. As previously [Heimann and Keeling, 1989], this analysis depends more on the correctness of atmospheric observations than on the inversion procedure used, because we invoke *a priori* information as far as practicable to reduce dependence on the inversion process. In Articles III and IV we assess how far we may trust these *a priori* choices and our input atmospheric data.

Below we describe the atmospheric transport model and *a priori* sources and sinks chosen for our regional analysis of the global carbon cycle. Except as noted below, we retain the isotopic methodology of Heimann and Keeling [1989], although with far more extensive use of isotopic data than previously.

2. General Strategy to Model the Global Carbon Cycle

Our objective is to simulate the observed seasonal cycle and interannual variations in atmospheric CO_2 by a correct choice of sources and sinks. Exchanges of atmospheric CO_2 with terrestrial and oceanic carbon reservoirs are defined by a set of boundary fluxes in an atmospheric transport model that predicts the time-varying concentration and $^{13}C/^{12}C$ ratio of atmospheric CO_2 from a knowledge of wind and turbulent motion. By adjusting the strengths of these boundary fluxes, the model predicts both the seasonal cycle of atmospheric CO_2 and its nonseasonal spatial distribution as functions of spatial coordinates and time, thus allowing a close match to observations of atmospheric CO_2.

The boundary fluxes are defined, in so far as possible, from prior knowledge of terrestrial and oceanic processes, expressed as spatially resolved source components, representing identifiable processes such as photosynthesis and respiration of plants and gas exchange between the atmosphere and the surface ocean. Some components are fully specified from *a priori* information, while others are adjusted by an optimal fitting procedure to predict the observed atmospheric CO_2 concentration and $^{13}C/^{12}C$ ratio. The transport model that makes this prediction solves the three-dimensional continuity equation of a passive atmospheric tracer.

The atmospheric data used in this study extend over a time-interval long enough to discern interannual variability in the carbon cycle in some detail. Ideally, and for consistency, such computations should be provided with detailed time-series data for all parameters that vary in time. Such data were not uniformly available, however, and we adopted a limited strategy focused on the variability in CO_2 exchange fluxes implied by our atmospheric CO_2 data. We used daily observations of wind for a single year, and multi-year averages of the seasonal cycle of net primary production (NPP) of plants, of heterotrophic respiration of plants and soil, and of physical oceanic processes. For wind fields, NPP, and fossil fuel emissions for which time-series were available for some or all years of our study (1981-1999), we carried out sensitivity tests to assess the effect of neglecting to consider their interannual variability.

We first describe the transport model, then the essential properties of the model source components and the fitting procedure by which time-dependent fluxes are derived. In two appendices we present details of the protocols for establishing these components and for carrying out fits to atmospheric data. We conclude with a brief discussion of the significance of the fluxes simulated by this inverse calculation.

3. Description of the Atmospheric Transport Model

To compute atmospheric CO_2 transport, we have adopted the three-dimensional transport model, TM2, of Heimann [1995], driven by meteorological observations. For our main calculations, the model was supplied with air-mass fluxes and subgridscale transport (hereafter together referred to as "operational analysis fields") for the calendar year 1986, processed by means of the analysis and forecasting system of the European Center for Medium-Range Weather Forecasts (ECMWF) [Bengtsson et al., 1982; Hollingsworth et al., 1985; ECMWF, 1999]. The data, at 12-hour intervals, were subsequently further processed by us for the TM2 grid, at a latitudinal spacing of 180°/23 (Table 1) and a longitudinal spacing of 10° (latitudinal spacings beginning at 0°, longitudinal at 5°). Advective transport was computed in three dimensions using the slopes scheme of Russell and Lerner [1981]. Subgridscale vertical transport was computed using the mass flux scheme of Tiedtke [1989]. Turbulent vertical transport due to stability-dependent vertical diffusion was calculated according to the scheme of Louis [1979]. The TM2 model employs 9 layers in the vertical dimension [Heimann, 1995], as shown in Table 2. The numerical time step is 4 hours.

For each model source component, TM2 was run with the ECMWF operational analysis fields repeated over the same annual cycle four times, as described by Heimann and Keeling [1989]. The results of the fourth year were extracted for selected locations by bilinear interpolation of longitude and sine of latitude and were subsequently decomposed for each location into a linear trend and four harmonics. The fourth year model results were used in the inverse calculation, providing a "quasi-stationary" approximation to interannual variability in transport and CO_2 sources and sinks. More details are given in Appendix A, section 1.

The bilinear horizontal interpolation procedure, used previously by Heimann et al. [1989], takes account of the model predictions of atmospheric CO_2 concentration and $^{13}C/^{12}C$ ratio for the grid box in which the station is located and for the three grid boxes contacting the boundaries of the quadrant

TABLE 1
LATITUDINAL COORDINATES OF THE THREE-DIMENSIONAL ATMOSPHERIC CO_2 TRANSPORT MODEL[a]

Zonal Index No.	Mid-Zone	Southern Boundary	Location of Adjustable Source Components	
			Biospheric	Oceanic
24	90.00 N.	86.09 N.	BIO4	OCE3
23	82.17 N.	78.26 N.	BIO4	OCE3
22	74.35 N.	70.43 N.	BIO4	OCE3
21	66.52 N.	62.61 N.	BIO4	OCE3
20	58.70 N.	54.78 N.	BIO4	OCE3
19	50.87 N.	46.96 N.	BIO4	OCE3
18	43.04 N.	39.13 N.	BIO3	OCE3
17	35.22 N.	31.30 N.	BIO3	OCE3
16	27.39 N.	23.48 N.	BIO3	OCE3
15	19.57 N.	15.65 N.	BIO2	OCE2
14	11.74 N.	7.83 N.	BIO2	OCE2
13	3.91 N.	0.00	BIO2	OCE2
12	3.91 S.	7.83 S.	BIO2	OCE2
11	11.74 S.	15.65 S.	BIO2	OCE2
10	19.57 S.	23.48 S.	BIO2	OCE2
9	27.39 S.	31.30 S.	BIO1	OCE1
8	35.22 S.	39.13 S.	BIO1	OCE1
7	43.04 S.	46.96 S.	BIO1	OCE1
6	50.87 S.	54.78 S.		OCE1
5	58.70 S.	62.61 S.		OCE1
4	66.52 S.	70.43 S.		OCE1
3	74.35 S.	78.26 S.		OCE1
2	82.17 S.	86.09 S.		OCE1
1	90.00 S.			

[a] Model grid boxes each have an extent of 180/23 degrees latitudinally, except the polar boxes, which are centered on the poles and have a meridional extent of 180/46 degrees.

of the grid box in which the station is located. The four magnitudes for concentration and $^{13}C/^{12}C$, are assumed to apply to the centers of their respective grid boxes. First, the easterly and westerly boxes are interpolated to the latitude of the station, and then these interpolated values, are interpolated to its longitude. This interpolation scheme effectively increases the coarseness of the spatial resolution of the model to twice the latitudinal and longitudinal dimensions of the grid boxes.

The urban location of our station at La Jolla, California poses a problem for use of the transport model, because of its proximity to large terrestrial CO_2 fluxes from fossil fuel combustion and exchange with the biosphere, a condition absent at all of the other sampling sites of our station array. By means of sensitivity tests described in Article 3, subsection 5.3, we establish that the inversion model results are sensitive to the exact manner of distributing model sources and sinks near this site. To reduce this sensitivity we have modified the distribution of sources and sinks in a preferred inversion calculation by removing all land-based CO_2 fluxes from the grid box in which La Jolla is located (see Article III, subsection 8.3).

To challenge the validity of the quasi-stationary approximation, we devised a more correct, extended response mode of calculation, described in Appendix B, that takes account of atmospheric CO_2 transport over 3 years preceding the year of simulation. As described in Article III, simulated short-term interannual fluctuations in CO_2 flux are slightly larger than in the quasi-stationary calculations reported here, but longer term trends change but little. Also described in Article III is a sensitivity test in which we used ECMWF operational analysis fields for 1987 in place of 1986 fields to assess for a pair of years the influence of interannually-varying atmospheric mass transport. In addition, we compared the result of replacing operational analysis fields for 1986 with ECMWF meteorological reanalysis fields [Gibson et al., 1997], for a sequence of years, 1979-1993. These reanalysis fields were produced by a version of the ECMWF analysis and forecasting system consistent for all years of the data set, which however required use of a newer transport model, TM3, having revised daily convection fields, and hybrid, rather than sigma, model levels. We were not able to implement these convection fields and, for all years of this multi-year simulation, we substituted monthly-averaged convection fields derived from the daily operational analysis fields of 1986, used for our main calculations.

The TM2 model has no explicit turbulent planetary boundary layer (PBL) and therefore predicts for the seasonal biospheric source component a lesser mean annual latitudinal gradient than do models with a PBL [cf. Denning et al., 1995; Law et al., 1996]. In Article III, subsection 2.4, by a comparison of predicted and observed vertical gradients in the far north where the PBL is most pronounced, we show evidence that TM2 provides a nearly correct result in spite of its lacking an explicit PBL formulation.

4. DESCRIPTION OF THE MODEL SOURCE COMPONENTS

4.1 Introduction

From atmospheric CO_2 data, described in Article I, only broad scale zonal variations in biospheric and oceanic CO_2 exchanges with the atmosphere are resolved in this study. Although, in principle regional fluxes could be computed for almost as many zones as there are stations in our array, such a calculation is ill-conditioned, because exchange fluxes vary with latitude in proportion to the difficult-to-determine second spatial derivative of the scalar fields of concentration and isotopic ratio [Bolin and Keeling, 1963].

To achieve a stable calculation we resolve fluxes for only three climatic zones, roughly identified as tropical, temperate, and polar. This choice presents us with 5 zones, one tropical and two extratropical zones in each hemisphere. The zones are defined to conform to the grid spacing of the TM2 model (see Table 1). The inversion computation is further stabilized [cf. Heimann and Keeling, 1989] by assigning realistic regional patterns to the source components, either fixed patterns or patterns which vary seasonally or interannually. The inversion process is thus reduced to adjusting a subset of these components, as described below. The success of this procedure depends on the correctness of both the transport model, TM2, and of the prescribed patterns and parameters pertaining to these source components.

4.2 Components and their isotopic representations

Eleven source components are established *a priori* and 7 others are adjusted during the inversion process to produce

TABLE 2

VERTICAL COORDINATES OF THE THREE DIMENSIONAL ATMOSPHERIC TRANSPORT MODEL

Model	Model levels (σ coordinate)		Global mean pressure levels (hPa)[a]			Geopotential
Level	Boundary	Delta	Boundary	Delta	"Mean level"	Height (km)[b]
	0.000000		10			26.2
9		0.0616		60	27	22.3
	0.061602		70			17.8
8		0.0821		80	103	15.7
	0.143737		150			13.6
7		0.1078		105	201	11.8
	0.251540		255			10.2
6		0.1386		145	321	8.7
	0.390144		390			7.3
5		0.1643		160	468	5.9
	0.554415		550			4.7
4		0.1745		170	634	3.6
	0.728953		720			2.6
3		0.1376		134	786	1.9
	0.866530		854			1.2
2		0.0821		80	894	0.8
	0.948665		934			0.4
1		0.0513		50	959	0.2
	1.000000		984			0.0

[a] Boundaries of global mean pressure levels are computed from corresponding σ values using $p = p_{top} + \sigma(p_s - p_{top})$, where p_s, the global average surface pressure, is taken to be 984 hPa and the topmost boundary of the model, p_{top}, is fixed at 10 hPa.

[b] Approximate heights above sea level are computed from the global mean pressure levels assuming a uniform lapse rate of 6.5 K km^{-1} and a global average surface temperature of 293°K [Heimann and Keeling, 1989, Table 2].

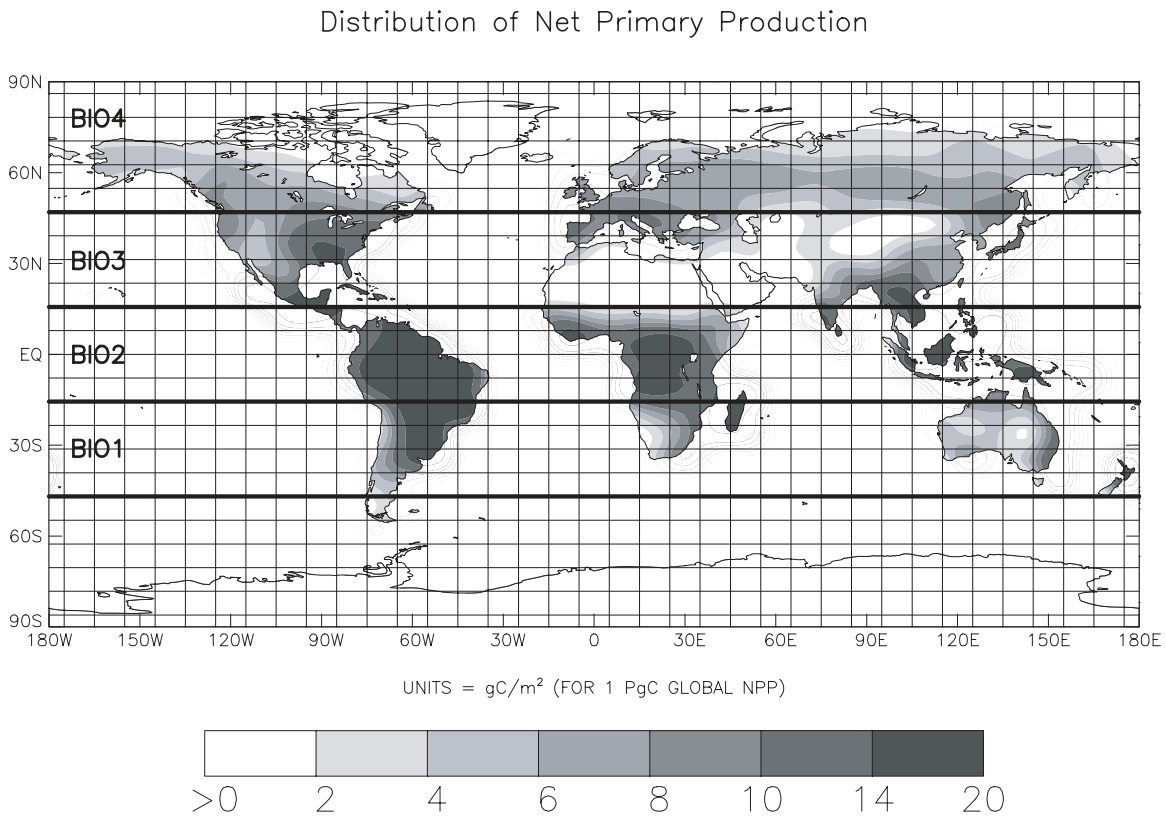

Fig. 1. Spatial distribution of annual net primary production (NPP) in gC m^{-2} yr^{-1} over land, averaged from 1982 through 1990. This distribution applies to the adjustable biospheric source components, BIO1-BIO4, as labeled within the zones distinguished by thick black lines and specified in Table 1. NPP was calculated from Pathfinder NDVI vegetative index data at a spatial resolution of 1° x 1°, regridded to the 8° x 10° resolution of the TM2 transport model, as described in the text, and was then contoured. The distribution is normalized to a global flux of 1 PgC yr^{-1}.

agreement with atmospheric CO_2 data. The 11 *a priori* components, listed in Table 3 with a 3-letter code, are essentially as described by Heimann and Keeling [1989]. Of these, 3 vary interannually in accord with results of the global single deconvolution calculations described in Article I, 6 vary only seasonally, 2 are invariant. (One additional interannually variable component, BSU, the "biospheric Suess effect", is provided for implicitly.) The 7 adjustable components, listed in Table 3 with a 3-letter code followed by a number, vary interannually.

Of the *a priori* source components, two are exclusively anthropogenic releases of CO_2 into the atmosphere: industrial emissions (code: IND) and a CO_2 terrestrial biospheric flux ("biospheric destruction") owing to land-use changes and deforestation (DES). Two others depict responses to these anthropogenic sources: terrestrial uptake of CO_2 by land plants, stimulated by higher concentrations of CO_2 in the ambient air (FER), and oceanic uptake of CO_2 caused by higher partial pressure of CO_2 in the air adjacent to the sea surface (EXC). On a global scale, these four components relate to annual average fluxes of the double deconvolution calculations of Article I: respectively, the two anthropogenic sources, IND and DES to F_{ind} and F_{des}, and the two responses, FER and EXC, to F_{fer} and F_{ex}. All except DES vary interannually.

The remaining *a priori* source components, disregarding those exclusively isotopic, described below, depict predominantly natural processes assumed not to vary interannually. These include two seasonally varying terrestrial fluxes which, combined, produce a zero net annual flux at every model grid point: net primary production (NPP) and heterotrophic respiration of the terrestrial biosphere (RES). One natural oceanic component (TDE), zero at every grid point over the annual cycle, varies with season as a function of seasurface temperature. Another oceanic component is a sink of atmospheric CO_2 northward of 23.5°N in the Atlantic Ocean, balanced globally by a zonal source southward of 39.1°S (ATL); it is seasonal only to the extent that air-sea exchange varies as a function of wind speed, a prescription that applies to all of the oceanic source components, as discussed below.

The seven adjustable components make use of factors that set their annual average strengths so as to predict optimally atmospheric CO_2 concentration and isotopic ratio. Each component occupies one or more of the 5 climatic zones of the transport model. Three components represent exchange with the oceans: southern extratropical (OCE1), tropical (OCE2), and northern extratropical (OCE3) where "extratropical" refers to temperate and polar zones combined. Four components represent exchange with the terrestrial biosphere: southern temperate (BIO1), tropical (BIO2), northern temperate (BIO3), and north polar (boreal) (BIO4). The Atlantic component, ATL, as noted above, is not adjustable, although it was in the earlier study of Heimann and Keeling [1989]. The three oceanic components sum to the global flux, $F_{ano,oce}$ and the four biospheric components sum to the global flux, $F_{ano,bio}$, these global fluxes defined in Article I, subsection 4.1.

Within each zone, each terrestrial biospheric source component, except biospheric destruction (DES), is distributed in proportion to the annual average of net primary production of land plants (NPP), determined at a resolution of 1° by 1° from 8-11 day composited values of a normalized difference vegetative index (NDVI), derived from remotely sensed radiometric data as compiled by the Pathfinder Project [James and Kalluri, 1994] and monthly average photosynthetically-active radiation (PAR) for 1986 and a constant quantum efficiency factor. The data were subsequently averaged from 1982 through 1990, and regridded to the 8° by 10° resolution of the TM2 model, as shown in Figure 1. Zonal and global totals of NPP are listed in Article I, Table 5.

The global total of NPP, 61.3 PgC yr^{-1}, is slightly greater than 55.9 PgC yr^{-1} found in a similar analysis by Heimann and Keeling [1989, p. 251] (Article I, Table 5). The distribution of heterotrophic respiration (RES) is determined by setting its annual average equal to that of NPP at the 1° by 1° resolution of the original calculations. Biospheric destruction is distributed in accordance with a study by Houghton et al. [1987], as described in Appendix A.12. Each oceanic source component, at 8° by 10° resolution, is distributed in proportion to a CO_2 gas exchange coefficient, and thus prescribed to vary seasonally (Figure 2). The equatorial oceanic component, OCE2, is also a function of an imposed fixed pattern in the air-sea partial pressure difference ΔpCO_2 (Figure 3), as determined by Heimann and Keeling [1989, Figure 10].

The isotopic specifications of the source components, three exclusively isotopic, are as described by Heimann and Keeling [1989]. The latter depict exchanges associated with isotopic disequilibria between the atmosphere and the oceanic and biospheric carbon pools caused by the addition of CO_2 to the atmosphere by fossil fuel combustion (OSU and BSU, respectively), and with temperature-dependent equilibrium fractionation at the atmosphere-ocean interface (TDF).

We do not include terrestrial source components representing afforestation [Houghton et al., 1994], nitrogen fertilization [Townsend et al., 1996; Holland et al., 1997], or biomass burning [Hao and Liu, 1994; Iacobellis et al., 1994]. The magnitudes of these fluxes are poorly established in both space and time. In combination, they are accounted for approximately in our study by the adjustable zonal terrestrial components, BIO1 to BIO4. Unidentified oceanic exchanges are similarly accounted for by the adjustable oceanic components, OCE1 to OCE3.

5. Atmospheric Input Data

The measurements of atmospheric CO_2 concentration and $^{13}C/^{12}C$ isotopic ratios used in this study were obtained from an array of 9 stations extending from the Arctic at 82°N to the South Pole. Concentration data are expressed as a mole fraction in parts per million of dry air (ppm), isotopic data in per mil (‰) by the reduced isotopic ratio, $\delta^{13}C$ defined by equation (A.4) in Appendix A, below. Data for one station, Mauna Loa Observatory, are not used directly, because locally varying winds, not captured by the coarse grid of the TM2 transport model, make it difficult to simulate data for this station, situated 3400 meters above sea level on the volcanic island of Hawaii. The nearby coastal station at Cape Kumukahi also provides data for the region, however. In Article IV, as a

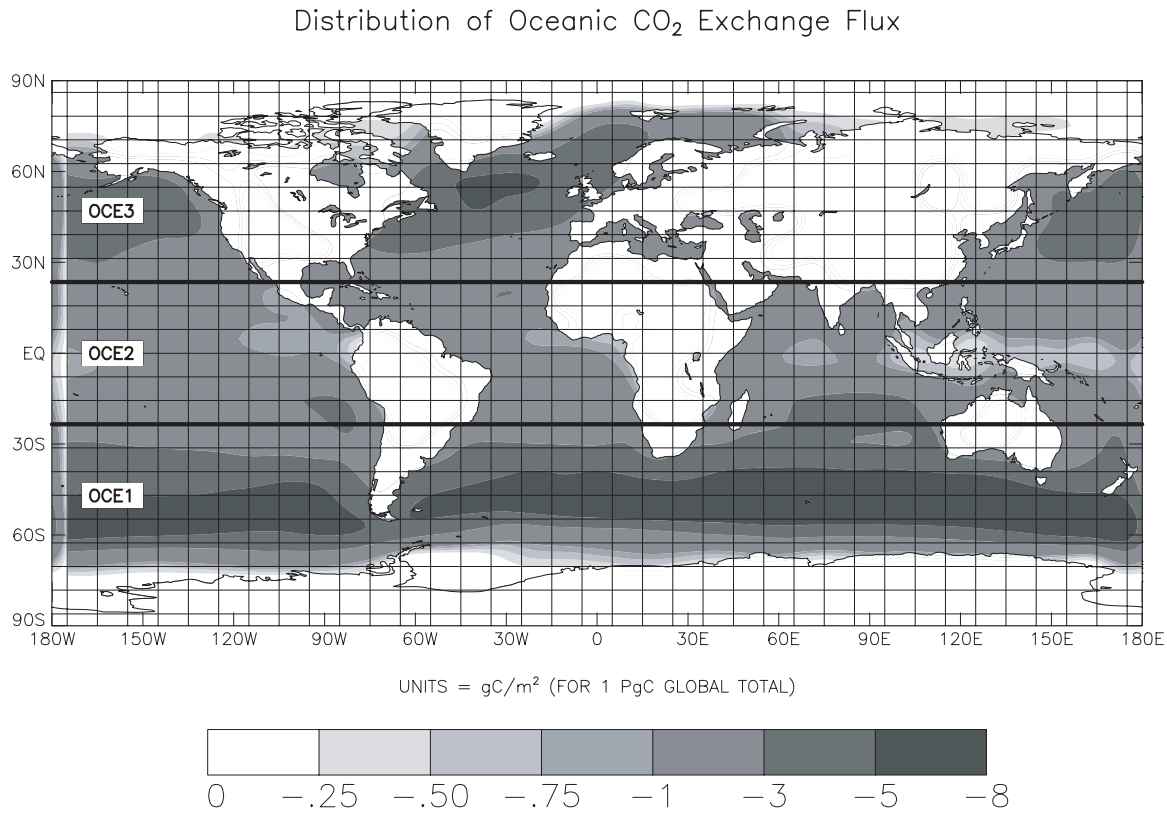

Fig. 2. Spatial distribution of the net annual oceanic exchange of atmospheric CO_2, as determined at a spatial resolution of 8° x 10° assuming a constant CO_2, partial pressure difference between the ocean-surface and the atmosphere, and the time- and space-dependent CO_2, gas exchange of Heimann and Monfray [1989]. The distribution applies to the adjustable source components, OCE1-OCE3, as labeled within the zones distinguished by thick black lines and specified in Table 1. The distribution is contoured and normalized to a global uptake flux of 1 PgC yr^{-1}; it applies directly to components, OCE1 and OCE3, but is modified for component OCE2, as indicated in Figure 3, below.

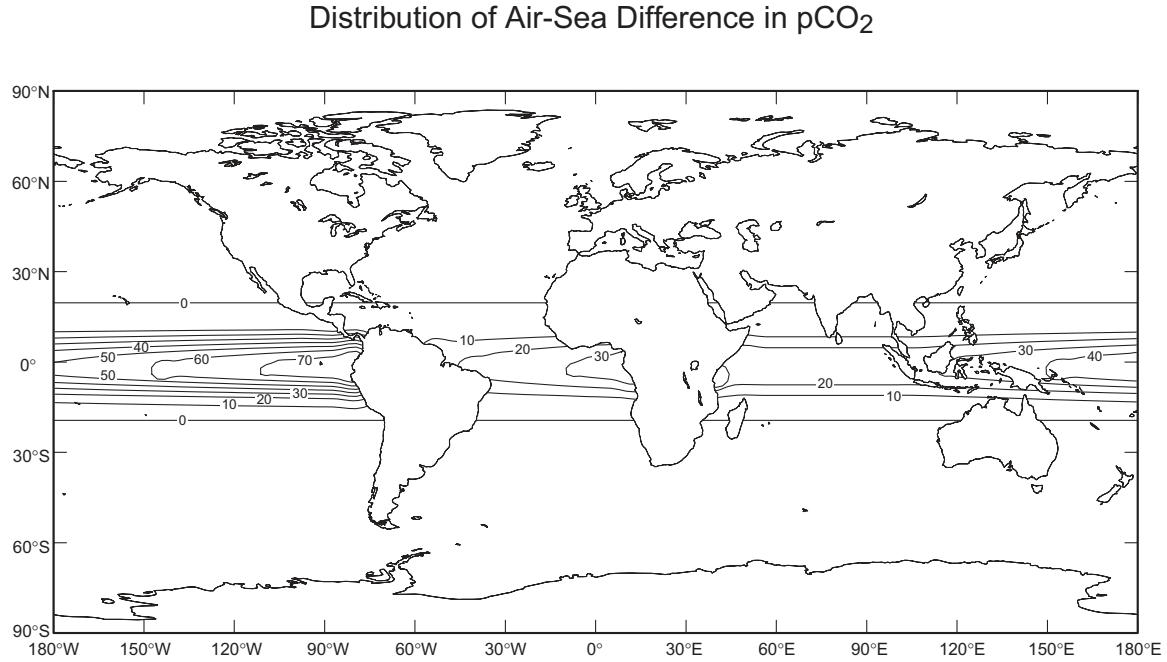

Fig. 3. Spatial distribution of the CO_2, partial pressure difference between the ocean-surface and the atmosphere, in μatm. This component applies to the adjustable tropical oceanic source component, OCE2, distributed in proportion to both this distribution and that shown in Figure 2. The partial pressure, as shown, is normalized to a zonal uptake of 1 PgC yr^{-1}, taking account of both distributions.

TABLE 3

SOURCE COMPONENTS OF THE ZONAL INVERSION MODEL

Source Component	Definition	Determination of Magnitude	Category[a]	Time Dependency Seasonal[b]	Interannual	Balanced	Corresponding Deconvolution Flux
Industrial:							
IND[c]	Industrial CO_2 release	*a priori*	anthropogenic	D	yes	no	F_{ind}
Biospheric:							
NPP	Net primary production of land plants	*a priori*[d]	natural	NPP	no	locally[e]	
RES	Heterotrophic respiration of land plants and soil	*a priori*[d]	natural	T	no	locally[e]	
FER	Terrestrial biospheric fertilization	*a priori*	anthropogenic	NPP	yes	no	F_{fer}
DES	Terrestrial biospheric destruction	*a priori*	anthropogenic	no	no	no	F_{des}
BIO1	Net terrestrial sink, 23.5-47°S	by adjustment	natural	NPP	yes	no	$F_{ano,bio}$
BIO2	Net terrestrial sink, 23.5°S-23.5°N	by adjustment	natural	NPP	yes	no	$F_{ano,bio}$
BIO3	Net terrestrial sink, 23.5-47°N	by adjustment	natural	NPP	yes	no	$F_{ano,bio}$
BIO4	Net terrestrial sink, 47-90°N	by adjustment	natural	NPP	yes	no	$F_{ano,bio}$
BSU[f,g]	Terrestrial flux to generate field C_{BSU} associated with the Suess Effect	*a priori*	anthropogenic	no	yes	no	
Oceanic:							
TDE	Seasonal CO_2 uptake and release by the oceans	*a priori*	natural	T,K	no	locally	
ATL	North Atlantic CO_2 uptake; release south of 39°S	*a priori*	natural	K	no	globally	
EXC	Uniform net oceanic sink for industrial CO_2	*a priori*	anthropogenic	K	yes	no	F_{ex}
OSU[f]	Oceanic flux to generate field C_{OSU}, associated with the Suess effect	*a priori*	anthropogenic	K	no	no	
TDF[f]	Flux for temperature-dependent fractionation	*a priori*	natural	T,K	no	globally	
OCE1	Net oceanic sink, 23.5-90°S	by adjustment	natural	K	yes	no	$F_{ano,oce}$
OCE2	Net oceanic sink, 23.5°S-23.5°N	by adjustment	natural	K	yes	no	$F_{ano,oce}$
OCE3	Net oceanic sink, 23.5-90°N	by adjustment	natural	K	yes	no	$F_{ano,oce}$

[a] "Anthropogenic" and "natural" mean primarily anthropogenic and natural respectively.
[b] "D" denotes direct data (estimate of Rotty [1982]); "K", a function of the CO_2 gas exchange coefficient; "NPP", proportional to net primary productivity; and "T", a function of temperature.
[c] Two data sets, with spatial distributions for 1980 and 1990, respectively, are used in combination, as described in the text.
[d] Separate model fit to seasonality in CO_2 concentration at three northern stations: Point Barrow, La Jolla, and Cape Kumukahi.
[e] NPP and RES together are locally balanced.
[f] Isotopic only.
[g] BSU (**B**iospheric **SU**uess Effect) is accounted for implicitly in our isotopic specifications for RES and DES, as described in section A.14 of text.

diagnostic aid, data simulated by the inversion model for the Mauna Loa site are compared with observations.

The seasonal cycle of atmospheric CO_2 for each station is expressed by a set of four harmonics, as prescribed by Equation (2.1) of Article I. Seasonal data for Point Barrow, Alaska; La Jolla; and Cape Kumukahi for the year 1986 were used are inputs to the model to determine two global parameters, e and ν (cf. Appendix A, section A.10). Seasonal data for other stations were reserved for comparison with model predictions, discussed in Article III.

For the inverse calculations, seasonally adjusted data were used, as plotted in Figure 3 of Article I, Panels c, and d. Daily values, derived from spline fits after seasonal adjustments, were annually averaged at 6-months intervals, to create overlapping annual means. Standard errors for each overlapping time-interval were computed by dividing the standard error, established for the spline fit of the full record of each station, by the square root of the number of measurements of each interval, as described by Keeling et al. [1989a, p. 169].

Global net exchange fluxes of atmospheric CO_2 with the oceans and terrestrial biosphere, computed by a double deconvolution procedure, and as plotted in Article I, Figure 9, Panel b, are also inputs to the inverse calculation. They are inferred from globally averaged time-series derived from the same CO_2 concentration and $^{13}C/^{12}C$ ratio data used in the inversion calculation.

6. COMPUTATIONAL PROCEDURES

6.1 Fitting procedures

To deduce sources and sinks of atmospheric CO_2 from the magnitudes of the set of source components, just described, the first step is to compute "model solutions", accounting separately for the global dispersion of CO_2 of each component by means of transport model, TM2. Then, because the transport equation of TM2 is linear with respect to the concentration of non-reactive chemical tracers such as CO_2, the model solutions for the individual source components are summed to produce a composite model solution that can be compared with the observed concentration and $\delta^{13}C$ of atmospheric CO_2.

Linearity in the transport equation of TM2 applies separately to each isotope of carbon, and hence to both CO_2 concentration and $\delta^{13}C$ in the approximate used here to compute $\delta^{13}C$ from the $^{13}C/^{12}C$ ratio (cf. Heimann and Keeling, 1989, section 5). Therefore, any source component magnitude can be adjusted via a single factor that does not involve its prescribed spatial distribution nor its seasonal phasing. Optimal fits at annual intervals to atmospheric CO_2

observations are obtained simply by varying the source-magnitude factors of the adjustable source components, BIO1 to BIO4 and OCE1 to OCE3, because these factors apply directly to the model solutions of the individual components as well as to the components themselves. By a fitting procedure involving just the source-magnitude factors of these adjustable source components, we thereby achieve a mathematically stable inverse computation of sources and sinks consistent with observed spatial and temporal variability in atmospheric CO_2, without a need for repeated runs of the transport model for the same component. Details of the fitting procedures are given in Appendix B.

This inversion computation is preceded, however, by two preliminary procedures. In the first, a fit is made to predict optimally the observed seasonal cycle of atmospheric CO_2 at Point Barrow, Alaska; La Jolla, California; and Cape Kumukahi, Hawaii, three stations in the northern hemisphere with pronounced seasonal cycles produced mainly by the terrestrial biosphere. For this fit, unlike the subsequent fit to seasonally-adjusted values, we selected the values at the nearest grid point in order to obtain the model predicted concentration corresponding to a particular station location. Only data for 1986 are used in this procedure (one of two years for which direct wind data were available to us, as discussed above). To initiate this fit, the 7 adjustable source magnitude factors, described above, are assigned tentative values.

This preliminary fit provides estimates of two adjustable global parameters that reflect the predicted metabolic activity of land plants and soils: an efficiency factor, e, that defines the amount of carbon fixed in photosynthesis per quantum of light energy, and a factor, ν, that defines the sensitivity of heterotrophic respiration to surface air temperature, as described in Appendix A, subsection A.10. With tentative values assigned to e and ν, a provisional optimal fit is made to the seasonally adjusted CO_2 and $^{13}C/^{12}C$ data of 1986 for all 9 stations used directly in our study, providing revised estimates of the 7 adjustable flux magnitudes, and two global constants, representing background levels of CO_2 concentration and isotopic ratio. The two procedures are then iterated. This is necessary because seasonal sources and sinks to some degree covary with seasonally variable atmospheric transport [Keeling et al., 1989b]. In practice, the two fits are nearly independent, however, giving satisfactory convergence at the second iteration. With e and ν thus established, optimal fits of the 7 adjustable source magnitude factors at 6-month intervals complete the inversion process.

To determine optimal fits at each iteration, we used a multiple linear regression procedure [Draper and Smith, 1981], weighted by observational errors and modified to incorporate constraints imposed by the global average terrestrial and oceanic fluxes found by the double deconvolution described in Article I. The first fit, which is seasonal, comprises one equation for each station, giving a system of 3 equations with 2 unknowns. The second, seasonally adjusted, fit comprises 2 equations per station, giving altogether a system of 18 equations in 7 unknowns (7 adjustable magnitudes and 2 background constants, less 2 deconvolution constraints). Details are given in Appendix B.

6.2 Errors estimated by Monte Carlo analysis

We performed Monte Carlo simulations to assess uncertainties in the zonally averaged fluxes introduced by uncertainties in the atmospheric observations of CO_2 and $^{13}C/^{12}C$ ratio and in the global constraints determined from the atmospheric observations via the double deconvolution. For each of the original observations of CO_2 and $^{13}C/^{12}C$, a corresponding random data point was created using a random number generator, specified to give a statistically normal distribution having the same mean and standard deviation as the observations [Press et al., 1992, pp. 271, 280, functions RAN1 and GASDEV]. One standard deviation (1σ) for the global oceanic and biospheric constraints was taken to be 0.5 PgC yr^{-1}, in general agreement with estimates by Keeling et al. [1995]. (We have confirmed that this estimate is approximately correct by an updated calculation, based on the average of atmospheric CO_2 data of Mauna Loa Observatory, Hawaii, and the South Pole from 1978 through mid-2000, which yields a σ of 0.39 PgC yr^{-1}.) The error in the global oceanic and biospheric constraints was assumed to be negatively correlated as was assumed in the error analysis of Keeling et al. [1995]. The inverse calculation was then performed on the new data set. This procedure was repeated 1000 times, resulting in a nearby normal distribution from which σ was determined.

6.3 Computation of reduced chi-square

As a further measure of the reliability of estimated fluxes, we computed reduced chi-square for individual annual model solutions, using the relation [Bevington, p. 188]

$$\chi^2_{red} = \frac{1}{\nu}\left(\sum_{j=1}^{l}(d_j/\sigma_j)^2 + \sum_{k=1}^{m}(d_k/\sigma_k)^2\right) \qquad (6.1)$$

where ν denotes the degrees of freedom, d_j the departure at observing station j from the observed annual mean CO_2 concentration, σ_j the associated standard error, d_k and σ_k corresponding factors for the reduced isotopic ratio, $\delta^{13}C$, and l denotes the total number of annual mean observations of both concentration and $\delta^{13}C$. For our standard case simulation of fluxes, the degrees of freedom are equal to the total number of observations, plus 2 global constraints minus the 9 following estimated variables: 4 adjustable biospheric fluxes, 3 adjustable oceanic fluxes, and one global constant each for CO_2 and $\delta^{13}C$. Reduced chi-square for longer periods was computed by averaging the reduced chi-square determined at 12-month time-steps.

7. Predicted Oceanic and Terrestrial Carbon Fluxes

The net atmospheric CO_2 oceanic and terrestrial biospheric exchange fluxes derived by inversion are plotted in the upper five panels of Figure 4 (thinner and thicker lines, respectively) for the five climatic zones distinguished in this study. Annual averages, overlapping at 6-month intervals are shown, plotted by connected line segments. Also, global totals of these fluxes, derived by double deconvolution prior to the inversion calculation, as described in section 5, above, are shown in the

bottom panel. The zonal fluxes in the upper five panels are forced to sum to these global fluxes by the fitting procedure of the inversion. Also plotted in the bottom panel is the sum of the global terrestrial and oceanic exchanges (very thick line).

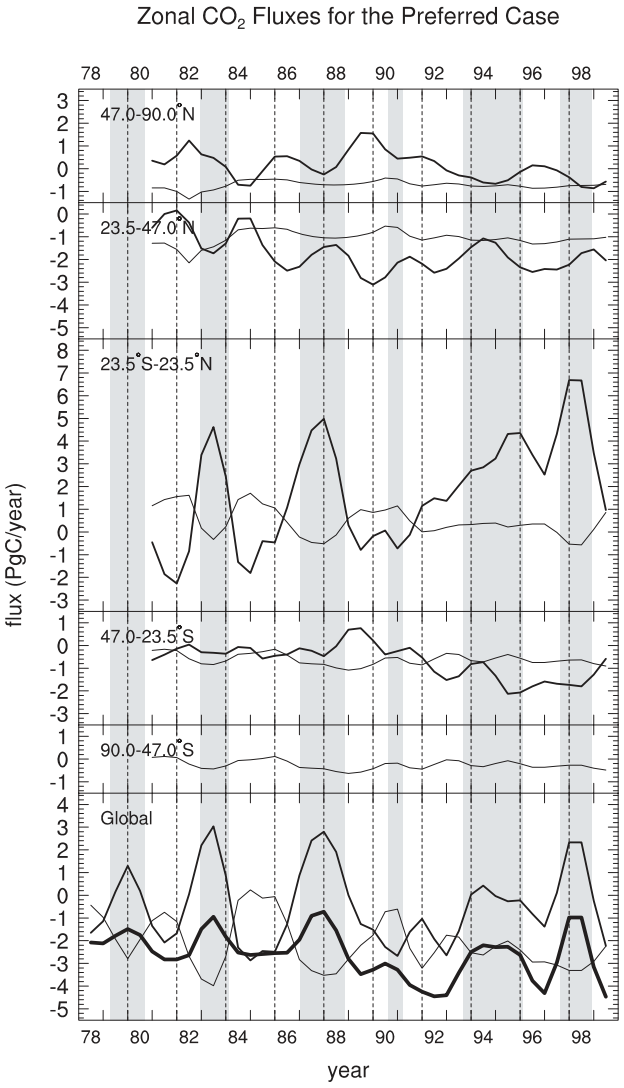

Fig. 4. Net annual CO_2, exchange fluxes, in PgC yr^{-1} positive to the atmosphere, calculated from data for atmospheric CO_2, concentration and $^{13}C/^{12}C$ isotopic ratio for a preferred model solution, as described in the text. Fluxes are shown for the terrestrial biosphere (thick line) and oceans (thin line) at 6-month intervals, for five latitudinal zones, consistent with the boundaries of the zones shown in Figures 1 and 2. Corresponding global terrestrial and oceanic fluxes that constrain this calculation, and their sum (extra thick line), are shown in the bottom panel. Gray bars demark approximately the times of El Niño events, inferred from time-intervals during which the rate of change of atmospheric CO_2, concentration at Mauna Loa Observatory, Hawaii, exceeded the trend in industrial CO_2, emissions, as shown in Figure 5 of Article I.

The most striking feature of the simulated fluxes shown in Figure 4 is a tendency of the terrestrial biosphere to be a substantial net source of atmospheric CO_2 in the northern polar zone and in the tropics, but a substantial sink in the northern mid-latitudes (23° – 47°N) between these zones. The tropical biospheric flux varies over the wide range of 8 PgC yr^{-1}, fluctuating strongly in the 1980's and then rising almost steadily to the highest value in the simulation in 1998. This pattern is almost mirrored in the global biospheric flux (bottom panel), consistent with the tropical biosphere being the primary origin of the large global excursions in atmospheric $^{13}C/^{12}C$ observed in our measurements on the El Niño time-scale.

In the northern polar zone, the terrestrial biospheric CO_2 source rises irregularly to a peak flux in 1989-1990 and afterwards declines. The peak is associated with unusually high CO_2 concentrations and negative $^{13}C/^{12}C$ ratios observed in 1989-1990 at the Point Barrow and Alert stations (see Figure 4 of Article I).

In temperate latitudes of both hemispheres, the terrestrial biosphere becomes progressively more of a sink of atmospheric CO_2 over time. Only in the southern hemisphere before 1990 is it sometimes a source, and then only weakly so.

The oceanic CO_2 fluxes vary considerably less than the terrestrial fluxes. They vary the most in the tropics in the 1980's, anti-correlated with the biospheric fluxes on the El Niño time scale. As was the case for the terrestrial biosphere, the pattern of tropical oceanic variations is similar to the global average flux, but with a lesser range of variability.

The estimated errors in these fluxes, caused by uncertainties in the atmospheric CO_2 observations (see subsection 6.2, above) are plotted in Figure 5. The errors, expressed as 2σ, range from as little as ± 0.2 PgC yr^{-1} for the southern oceanic zones to ± 1.0 PgC yr^{-1} for the tropical biosphere.

8. Discussion and Conclusions

Our findings suggest that substantial net sources and sinks of atmospheric CO_2 have prevailed over broad geographic zones during the past two decades. Here we present an initial consideration of these findings, reserving for Articles III and IV, a more detailed analyses.

The best established finding is a global CO_2 sink created jointly by the global net biospheric and oceanic fluxes. As discussed in Article I, the calculation of this combined sink depends only on the precisely determined globally averaged atmospheric CO_2 concentration and on release of CO_2 from industrial sources; it has fluctuated from year to year since 1978 by nearly 4 PgC yr^{-1} (very thick curve in the bottom panel of Figure 4); it is weakest during climatic events, whose durations are approximately as shown by vertical gray bars (see Article I, subsection 2.2). The greatest swing in its strength over the record period occurred in association with an El Niño event in 1998. Little of this variation is due to industrial CO_2 emissions, known to be only slowly varying.

Less well established, because variability in the $^{13}C/^{12}C$ isotopic discrimination of photosynthesis on land is uncertain, are computed variations in the separate global terrestrial and oceanic fluxes (lowest panel of Figure 4). If our assumption of constant discrimination is correct, fluctuations in the terrestrial flux not only explain most of the variability of the combined flux, but are so large as to require a nearly opposite pattern of variation in the global oceanic flux.

This inferred opposition of global fluxes is reduced, or disappears, if isotopic discrimination during photosynthesis diminishes during El Niño events. As discussed in Article

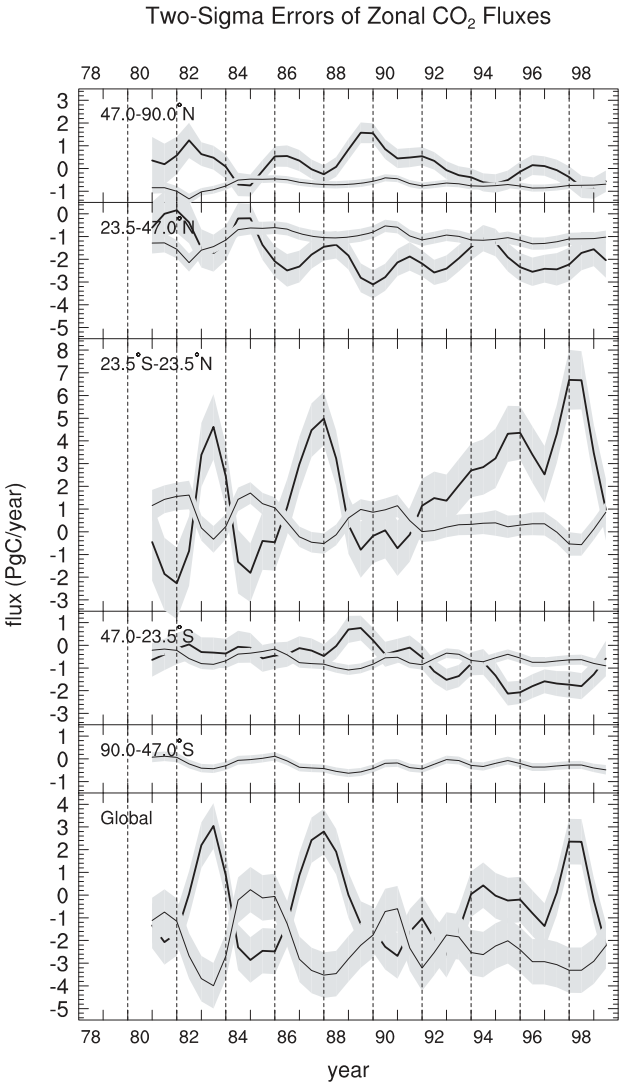

Fig. 5. Standard errors (2σ), in PgC yr^{-1}, shown by gray shading, for the terrestrial biospheric and oceanic fluxes shown in Figure 4. These errors, established by a Monte Carlo procedure, are owing to uncertainty in observations of atmospheric CO_2 concentration and $^{13}C/^{12}C$ isotopic ratio, and to uncertainty in the computed global terrestrial and oceanic fluxes that constrain the regional fluxes.

I, the close phasing of the $^{13}C/^{12}C$ and CO_2 concentration signals of atmospheric CO_2 requires that changes in discrimination be closely in phase with the El Niño cycle, in order that the terrestrial and oceanic fluxes sum to the well determined combined sink (very thick curve in the lowest panel of Figure 4). As is evident (see upper five panels of Figure 4), terrestrial and oceanic fluxes show a strong relation to El Niño events only in the tropical zone where their temporal patterns are similar to the corresponding global fluxes. As discussed in Article IV, subsection 5.4, warmer and drier conditions than otherwise in this zone during Niño events may bring about reduced isotopic discrimination that is linked to reduced photosynthesis of land plants, both phenomena caused by drought stress. If so, we may have falsely simulated opposing terrestrial biospheric and oceanic fluxes, in spite of striking similarity in phasing of the fluctuations in atmospheric CO_2 concentration and $^{13}C/^{12}C$ ratio.

In summary, from inverse analysis of our observational data, we find evidence of strong interannual variability in terrestrial biospheric fluxes. Our findings are sensitive to our isotopic data mainly to establish the decadal average strengths of zonal sources and sinks in each zone and, in the tropical zone, extremes in the terrestrial biospheric and oceanic fluxes linked to the El Niño cycle.

APPENDIX A
SPECIFICATION OF MODEL SOURCE COMPONENTS

A.1 Introduction

Our general goal is to identify exchange fluxes of CO_2 between the oceans, terrestrial biosphere and the atmosphere that explain the observed distributions of atmospheric CO_2 concentration and isotopic ratio. The fluxes are specified as boundary conditions of the TM2 atmospheric transport model, the latter described in section 3 of the main text. The predictions are made for one annual cycle at a time, with interannual variability portrayed by variability in these cycles overlapped at 6-month intervals.

We follow the approach of Heimann and Keeling [1989] by defining a set of source components, $F_i\ (\mathbf{x}, t)$, as a function of time, t, in years, and of the three-dimensional space coordinate $\mathbf{x} \equiv x, y, z$ to represent CO_2 fluxes. The components, i, are expressed per unit area of land or ocean, as appropriate, and are defined as positive when the net transport is from the Earth's surface to the atmosphere. Annual averages are distinguished with a bar, thus

$$\overline{F_i}(\mathbf{x}, t) = \int_{t-\frac{1}{2}}^{t+\frac{1}{2}} F_i(\mathbf{x}, t')dt' \qquad \text{(A.1)}$$

Components declared to be invariant over the annual cycle are also labeled with a bar.

The total (or "composite") source flux, $F_{CMPS}(\mathbf{x}, t)$ is expressed by the sum of the source components

$$F_{CMPS}(\mathbf{x}, t) = \sum_{i=1}^{n} F_i(\mathbf{x}, t) \ \ [4.1] \qquad \text{(A.2)}$$

(Equation numbers in brackets here refer to equivalent expressions of Heimann and Keeling [1989]). The transport model is run separately for each component, n in number, to produce a model solution ("model response"), $C_i(\mathbf{x}, t)$, that represents the computed incremental change in concentration of CO_2 corresponding to $F_i(\mathbf{x}, t)$. Because the basic transport model equation is linear with respect to tracer concentration, the composite model solution, $C_{CMPS}(\mathbf{x}, t)$, can be written

$$C_{CMPS}(\mathbf{x}, t) = \overline{C}_o(t) + \sum_{i=1}^{n} C_i(\mathbf{x}, t) \ \ [4.2] \qquad \text{(A.3)}$$

where $\overline{C}_o(t)$ denotes a background concentration of CO_2 which we set equal to the mean annual surface concentration at the South Pole. ($\overline{C}_o(t)$ thus varies with time only as inversions are performed for different time-intervals).

To compute isotopic ratios, we identify isotopic source components, ${}^*F_i(\mathbf{x}, t)$, and isotopic model solutions, ${}^*C_i(\mathbf{x}, t)$, corresponding to $F_i(\mathbf{x}, t)$ and $C_i(\mathbf{x}, t)$, but with respect to

the rare stable isotope, carbon-13, instead of to the sum of the stable isotopes of carbon, carbon-12 and carbon-13. We define a reduced isotopic ratio (cf. Article I, equation (1.1)) by the expression

$$\delta^{13}C = (r_j - r_s)/r_s \ \ [5.3] \tag{A.4}$$

where r_j and r_s denote the $^{13}C/^{12}C$ ratio of CO_2 in a carbon pool, j, and a standard ratio, respectively. We then compute an isotopic increment defined by

$$\Delta\delta_i(\mathbf{x},t) = \frac{(\delta_i(\mathbf{x},t) - \overline{\delta}_o(t))C_i(\mathbf{x},t)}{C_{CMPS}(\mathbf{x},t)} \ \ [5.17] \tag{A.5}$$

$\mathbf{x}$, and time, t, corresponding to the incremental change in concentration $C_i(\mathbf{x},t)$. In this expression $\delta_i(t)$ denotes $\delta^{13}C$ of the source component relative to a background isotopic ratio, $\overline{\delta}_o(t)$, corresponding to the background concentration, $\overline{C}_o(t)$. The difference, $\delta_i(t) - \overline{\delta}_o(t)$, generally reflects a known fractionation process.

The composite model solution for reduced isotopic ratio, analogous to equation (A.3) for CO_2 concentration, is therefore written

$$\delta_{CMPS}(\mathbf{x},t) = \overline{\delta}_o(t) + \sum_{i=1}^{n} \Delta\delta_i(\mathbf{x},t) \tag{A.6}$$

To establish $< \overline{\alpha}_{eq} >$, we computed $\alpha_{eq}(\mathbf{x},t)$ for each grid box of transport model TM2 and for each month, weighted by the exchange coefficient $k_{ex}(\mathbf{x},t)$. The resulting average, 0.990983, is 0.37‰ less than that used in the deconvolution model of Article 1.

We also take account of annual average reduced isotopic ratios of the carbon pools, $\overline{\delta}_a(t)$, $\overline{\delta}_b(t)$, and $\overline{\delta}_m(t)$, $\overline{\delta}_{ind}(t)$. which vary interannually, as listed in Article I, Table 4. Those of $\overline{\delta_a}(t)$ are from direct observations shown in Figure 3 of Article I. The values of $\overline{\delta}_b(t)$ and $\overline{\delta}_m(t)$ are based on the output of the single deconvolution calculations of Article I, and therefore take account of the Suess effect, described in subsections A.8 and A.14, below.

The equations relating these isotopic factors, as set forth below, are as derived by Heimann and Keeling [1989]. We have replaced the quotients $\overline{r}_a/r_s$ and $\overline{r}_m/r_s$ by their equivalents $(1+\overline{\delta}_a)$ and $(1+\overline{\delta}_m)$. The standard isotopic ratio, r_s, is listed in Article 1, Table 3. A factor R_s, that appears in some of the equations, denotes the ratio of ^{13}C to the sum of $^{12}C + {}^{13}C$ for the standard isotopic ratio, i.e.

$$R_s = r_s/(1 + r_s). \ \ [5.5] \tag{A.7}$$

A.2 Industrial Emissions: Source Component $F_{IND}(\mathbf{x},t)$

A single global source component, $F_{IND}(\mathbf{x},t)$, specifies the spatial distribution of industrial CO_2 released into the atmosphere by the combustion of coal, oil, and gas, gas flaring, and cement production; it is based on distributions for 1980 and 1990 given by Andres et al. [1996a,b, 2000] on a 1° by 1° grid. The seasonality of industrial emissions in each grid cell north of 23.5°N is expressed by a Fourier fit of 6 harmonics to monthly percentages of the annual total as determined by Rotty [1987] for 1982, and with opposite phase assumed south of 23.5°S. In the tropics, between these zones, emissions were assumed to be non-seasonal. The atmospheric CO_2 response was computed by transport model, TM2, for a hypothetical 1 PgC yr^{-1} source for the year 1980 and again for 1990. For all other years, in which distributions were unavailable, we calculated atmospheric responses by a linear interpolation in time of the 1980 and 1990 responses. Atmospheric responses were prorated to annual global source strengths specified by Boden et al. [1996].

The weighted average isotopic composition of the emissions is as specified by Andres et al. [1996c, 2000] applied globally, uniformly in space and time for each year. The isotopic increment (cf. equation (A.5)) associated with $F_{IND}(\mathbf{x},t)$ the industrial source is

$$\Delta\delta_{IND}(\mathbf{x},t) = (\overline{\delta}_{IND}(t) - \overline{\delta}_o(t))\frac{C_{IND}(\mathbf{x},t)}{C_{CMPS}(\mathbf{x},t)} \ \ [5.19] \tag{A.8}$$

where $\overline{\delta}_{IND}(t)$ denotes the global annual average $\delta^{13}C$ of CO_2 from industrial sources, and $C_{IND}(\mathbf{x},t)$ denotes the transport model response to the industrial source.

In Article III, we test the influence of a fossil fuel source for 1995 produced by Brenkert et al. [1998] on the basis of different national population estimates and coal carbon coefficients than used by Andres et al. [1996a,b] in producing the 1980 and 1990 distributions. Also, in Article III, we discuss the effect of accounting for latitudinal variations in the isotopic composition of industrial emissions, as specified in Andres et al. [1996c, 2000], instead of holding the isotopic composition globally uniform as we have in our standard source, described here.

A.3 General Oceanic Model Equations

Oceanic CO_2 exchange fluxes with the atmosphere are distributed in space and time within specified regions by the general equation

$$F_{OCD}(\mathbf{x},t) = k_{ex}(\mathbf{x},t)(pCO_{2\ sea}(\mathbf{x},t) - pCO_{2\ air}(\mathbf{x},t)) \ \ [4.20] \tag{A.9}$$

where the source component, $F_{OCD}(\mathbf{x},t)$, denotes a generalized net CO_2 flux, positive when directed into the atmosphere, and $\mathrm{pCO}_{2\ sea}(\mathbf{x},t)$ and $\mathrm{pCO}_{2\ air}(\mathbf{x},t)$ denote the associated partial pressures of CO_2 in the surface ocean and atmosphere, respectively. The label "OCD" indicates a component that is "oceanic concentration dependent," and therefore a function of $\mathrm{pCO}_{2\ sea}(t)$. This label is in contrast to those for several oceanic source components, discussed below, for which the CO_2 exchange affects only isotopic ratios. The CO_2 gas exchange coefficient, $k_{ex}(\mathbf{x},t)$, was evaluated as a function of wind speed and temperature expressed according to the parameterization of Heimann and Monfray [1989], in which monthly wind speeds were obtained partly from an ECMWF operational data set [Bengtsson et al., 1982; Hollingsworth et al., 1985] and partly from the Comprehensive Ocean-Atmosphere Data Set (COADS) [Woodruff et al., 1987]. Monthly sea surface temperatures were obtained from the Global Weather Experiment for the year 1979 [Bengtsson et al., 1982]. These data are treated as a climatological data set and, therefore, $k_{ex}(\mathbf{x},t)$ is assigned the same values,

$F_{ex}(\mathbf{x})$, for successive annual cycles. For the tropical oceanic component, the flux is specified as the product of $k_{ex}(\mathbf{x})$ and of the distribution of $\overline{\mathrm{pCO}_{2\ sea}}(\mathbf{x},t) - \overline{\mathrm{pCO}_{2\ air}}(\mathbf{x},t)$, as discussed in section A.5, below. For a component depicting seasonal air-sea exchange, discussed in section A.7 below, the oceanic partial pressure is assumed to vary seasonally. For all other oceanic components, the partial pressure difference is assumed to be constant over each specified region, hence the quantity $\overline{\mathrm{pCO}_{2\ sea}}(\mathbf{x}) - \overline{\mathrm{pCO}_{2\ air}}(\mathbf{x})$, is set to produce a desired annual net CO_2 flux for that region.

The isotopic increment associated with $F_{OCD}(\mathbf{x},t)$ is evaluated as a global annual average by the expression

$$\overline{\delta}_{OCD}(t) = \alpha_{am} < \overline{\alpha}_{eq} > (1 + \overline{\delta}_m(t)) - 1 \quad [5.57] \quad \text{(A.10)}$$

To arrive at values for reduced isotopic ratios, $\delta_i(\mathbf{x},t)$, of the source components, we take into account kinetic isotopic fractionation factors, α_{jk}, and an equilibrium isotopic fractionation factor, $< \overline{\alpha}_{eq} >$, listed in Article 3, Table 3. The kinetic factors denote isotopic fractionation attending the transfer of carbon from carbon pool j to k, where a denotes specifically the atmospheric carbon pool (or "reservoir"), b the terrestrial biospheric pool, and m the carbon pool of the surface "mixed" layer of the ocean. The equilibrium factor, $< \overline{\alpha}_{eq} >$, denotes a global annual average of a space and time-variable factor, $\alpha_{eq}(\mathbf{x},t)$, with respect to an isotopic equilibrium state between CO_2 gas residing in air and dissolved in seawater. In our calculations its interannual variability owing to variable temperature is disregarded. Possible slight interannual variability in the α_{jk} is also disregarded. In our computations α_{am} is fixed at 0.9982 (Article I, Table 4).

A.4 Perturbation Ocean Sink: Source Component $\overline{F}_{EXC}(\mathbf{x},t)$

The global annual average rate at which CO_2 from anthropogenic activities is taken up by the oceans, component $\overline{F}_{EXC}(\mathbf{x},t)$, is prescribed to be equal to the equivalent global flux, F_{ex}, as estimated by single deconvolution in Article I; it is distributed spatially in proportion to seasonally varying $k_{ex}(\mathbf{x},t)$ over the ice-free ocean surface. The isotopic increment associated with $\overline{F}_{EXC}(\mathbf{x},t)$ is given by

$$\Delta\delta_{EXC}(\mathbf{x},t) = (\overline{\delta}_{OCD}(t) - \overline{\delta}_o(t))\frac{C_{EXC}(\mathbf{x},t)}{C_{CMPS}(\mathbf{x},t)} \quad [5.58] \quad \text{(A.11)}$$

A.5 Adjustable Zonal Oceanic Source Components: $F_{OCE1}(\mathbf{x},t)$, $F_{OCE2}(\mathbf{x},t)$, $F_{OCE3}(\mathbf{x},t)$

Three adjustable source components for geographic zones are provided in the model to depict short-term interannual variations in major regions of the oceans. Only two of these are independent, however, because the components are forced to sum to the anomalous global perturbation flux, $F_{ano,oce}$, determined by double deconvolution, as described in Article I. The boundaries separating the three zones are set at 23.5°N and 23.5°S, to provide a tropical source component, $F_{OCE2}(\mathbf{x},t)$, and a northern and a southern extratropical source component, $F_{OCE3}(\mathbf{x},t)$ and $F_{OCE1}(\mathbf{x})$, respectively. All three are distributed in proportion to $k_{ex}(\mathbf{x},t)$. For $F_{OCE2}(\mathbf{x},t)$, the flux is set, in addition, to vary spatially in proportion to $\mathrm{pCO}_{2\ sea}(\mathbf{x},t) - \mathrm{pCO}_{2\ air}(\mathbf{x},t)$, determined by direct partial pressure measurements that indicate a net source of CO_2 to the atmosphere between 15.6°N and 15.6°S, with a characteristic time-invariant pattern as described by Heimann and Keeling [1989] and shown in Figure 3. From 15.6° to 23.5° in each hemisphere, a zero flux is assumed, roughly in agreement with observations. The pattern is assumed to be invariant in time, but the zonal total strength of the flux is adjusted in each inversion. The isotopic increment associated with the adjustable oceanic source components is

$$\Delta\delta_{OCEi}(\mathbf{x},t) = (\overline{\delta}_{OCD}(t) - \overline{\delta}_o(t))\frac{C_{OCEi}(\mathbf{x},t)}{C_{CMPS}(\mathbf{x},t)} \quad [5.58] \quad \text{(A.12)}$$

where i = 1, 2, or 3.

A.6 North Atlantic Sink: Source Component $\overline{F}_{ATL}(\mathbf{x},t)$

This oceanic component, $\overline{F}_{ATL}(\mathbf{x},t)$, which is not adjustable, takes into account transfer of CO_2 between the hemispheres produced by a CO_2 sink in the Atlantic Ocean north of 23.5°N, and a compensating source over the entire oceanic zone south of 39°S to achieve a zero net global source. This component is distributed in proportion to $k_{ex}(\mathbf{x},t)$. Our basis for including this component is an inverse calculation by Keeling et al. [1989b] indicating that the North Atlantic ocean was a sink of between 0.7 and 1.1 PgC per year for selected years between 1962 and 1984. Subsequent attempts to corroborate this source strength by direct oceanic observations have, however, all led to smaller estimates of the flux. A sink of about 0.6 PgC per year was estimated by Broecker and Peng [1992] on the basis of calculations of the carbon cycle of sea water monitored with pre-formed phosphate, while Watson et al. [1995] and R. F. Keeling and Peng [1995] estimated a sink of between 0.4 and 0.5 PgC per year to satisfy the atmospheric heat budget. As a compromise between these estimates, we assume a sink of 0.7 PgC per year. The choice of strength is not crucial to our model simulations, however, because the adjustable flux components, discussed above, compensate for error in its designated north-south distribution. We include $\overline{F}_{ATL}(\mathbf{x},t)$ in our set of source components because the adjustable oceanic components, being zonal, do not allow for a sink specifically in the north Atlantic ocean independent of the flux in the North Pacific Ocean. The isotopic increment associated with $\overline{F}_{ATL}(\mathbf{x},t)$ is

$$\Delta\delta_{ATL}(\mathbf{x},t) = (\overline{\delta}_{OCD}(t) - \overline{\delta}_o(t))\frac{C_{ATL}(\mathbf{x},t)}{C_{CMPS}(\mathbf{x},t)} \quad [5.58] \quad \text{(A.13)}$$

A.7 Seasonal Oceanic CO_2 exchange: Source Component $F_{TDE}(\mathbf{x},t)$

Following Heimann and Keeling [1989], we specified a purely seasonal CO_2 exchange source component between the atmosphere and the oceans, $F_{TDE}(\mathbf{x},t)$, having for each grid cell a zero net annual CO_2 exchange. Between 35.2°N and 35.2°S, $\mathrm{pCO}_{2\ sea}(\mathbf{x},t)$ is set to vary seasonally with temperature according to the chemical relationship of Weiss et

al. [1982]. Poleward, the temperature dependence is linearly reduced to zero at 50.9°, so as to account approximately for counteracting variations at higher latitudes caused by drawdown of surface oceanic CO_2 by photosynthesis of phytoplankton in spring and summer and vigorous mixing of deep water, high in CO_2, with surface waters in the winter. No attempt is made to model a seasonal exchange poleward of 50.9°, which is accordingly set to zero. The isotopic increment associated with $F_{TDE}(\mathbf{x},t)$ is

$$\Delta\delta_{TDE}(\mathbf{x},t) = (\overline{\delta}_{OCD}(t) - \overline{\delta}_o(t))\frac{C_{TDE}(\mathbf{x},t)}{C_{CMPS}(\mathbf{x},t)} \quad [5.58] \tag{A.14}$$

A.8 Oceanic ^{13}C Suess Effect: Source Component ${}^*\overline{F}_{OSU}(\mathbf{x},t)$

Oceanic carbon in subsurface waters to a large extent is not in isotopic equilibrium with the overlying atmospheric CO_2, because δ^{13}C of atmospheric CO_2 since the 1800's has been decreasing in response to the addition of anthropogenic CO_2 from fossil fuel emissions too rapidly to equilibrate with these waters. We refer to this disequilibrium as the "oceanic ^{13}C Suess effect" [Heimann and Keeling, 1989, eq. (5.43)]. We model it by an exclusively isotopic, annually averaged, source component

$$\begin{aligned}{}^*\overline{F}_{OSU}(\mathbf{x},t) =& k_{ex}(\mathbf{x},t)R_s\alpha_{am} < \overline{pCO}_{2\ air}(t) > \\ & (< \overline{\alpha}_{eq} > (1+\overline{\delta}_m(t)) - (1+\overline{\delta}_a(t))) \quad [5.52]\end{aligned} \tag{A.15}$$

The incremental change in CO_2 concentration associated with ${}^*F_{OSU}(\mathbf{x},t)$ is given by the expression

$$\overline{C}_{OSU}(\mathbf{x},t) = \frac{< \overline{pCO}_{2\ air} > (t)}{3.7609}\,\overline{C}_{EXC}(\mathbf{x},t) \quad [5.54] \tag{A.16}$$

The factor 3.7609 expresses the globally and annually averaged $\mathrm{pCO}_{2\ sea} - \mathrm{pCO}_{2\ air}$ required to produce a flux of 1 PgC yr^{-1} when multiplied by $k_{ex}(\mathbf{x},t)$ [Heimann and Keeling, 1989, p. 256]. The corresponding incremental change in δ^{13}C for a change in $C_{CMPS}(\mathbf{x},t)$ is given by the expression

$$\begin{aligned}\overline{\Delta\delta}_{OSU}(\mathbf{x},t) =& \alpha_{am}(< \overline{\alpha}_{eq} > (1+\overline{\delta}_m(t)) - \\ & (1+\overline{\delta}_a(t)))\frac{\overline{C}_{OSU}(\mathbf{x},t)}{C_{CMPS}(\mathbf{x},t)} \quad [5.55]\end{aligned} \tag{A.17}$$

A.9 Equilibrium Temperature-Dependent Fractionation: Source Component ${}^*\overline{F}_{TDF}(\mathbf{x},t)$

Temperature-dependent fractionation of ^{13}C and ^{12}C of CO_2 exchanged between the air and sea generates a $^{13}CO_2$ flux that is denoted by an isotopic source component, ${}^*\overline{F}_{TDF}(\mathbf{x},t)$, given by the expression

$$\begin{aligned}{}^*\overline{F}_{TDF}(\mathbf{x},t) =& k_{ex}(\mathbf{x},t)R_s\alpha_{am}(1+\overline{\delta}_m(t)) \\ & < \overline{pCO_{2\ sea}}(t) > (\alpha_{eq}(\mathbf{x},t) - < \overline{\alpha}_{eq} >) \quad [5.42]\end{aligned} \tag{A.18}$$

The partial pressure, $\overline{\mathrm{pCO}_{2\ sea}}$, for simplicity is set equal to the globally averaged partial pressure of CO_2 in the atmosphere, as specified by double deconvolution. The isotopic increment associated with ${}^*F_{TDF}(\mathbf{x},t)$ is

$$\overline{\Delta\delta}_{TDF}(\mathbf{x},t) = \frac{{}^*\overline{C}_{TDF}(\mathbf{x},t)}{C_{CMPS}(\mathbf{x},t)R_s} \quad [5.50] \tag{A.19}$$

The factor ${}^*\overline{C}_{TDF}(\mathbf{x},t)$ denotes the incremental change in $^{13}CO_2$ in the atmosphere generated by ${}^*F_{TDF}$. A separate computer run of transport model TM2 is required to determine this component, the only such run that involves an isotopic flux.

A.10 Seasonal Biospheric Exchanges: Source Components $F_{NPP}(\mathbf{x},t)$ and $F_{RES}(\mathbf{x},t)$

Exchange of CO_2 between the atmosphere and the terrestrial biosphere is simulated by a pair of strongly seasonally varying source components, by two fixed components, and by four adjustable components which vary slightly with season. Seasonal exchange is mainly specified by a flux component, $F_{NPP}(\mathbf{x},t)$, representing net primary productivity (NPP), and by a component, $F_{RES}(\mathbf{x},t)$, representing heterotrophic respiration.

The individual fluxes of this latter pair are locally balanced over the annual cycle, i.e.

$$\overline{F}_{NPP}(\mathbf{x},t) + \overline{F}_{RES}(\mathbf{x},t) = 0 \tag{A.20}$$

Thus, $\overline{F}_{RES}(\mathbf{x},t)$ is forced to be equal in magnitude to $\overline{F}_{NPP}(\mathbf{x},t)$ but opposite in sign. The latter flux is computed first, by the formula

$$F_{NPP}(\mathbf{x},t) = -e \bullet FPAR(\mathbf{x},t) \bullet PAR(\mathbf{x},t) \quad [4.3] \tag{A.21}$$

where e denotes a universal light efficiency factor, $PAR(\mathbf{x},t)$ photosynthetically-active radiation (PAR), and $FPAR(\mathbf{x},t)$ the fraction of PAR absorbed by plants. $PAR(\mathbf{x},t)$ was estimated from satellite observations by Pinker and Lazslo [1992] for the year 1986. We express FPAR(**x**,t) by a linear function of a normalized difference vegetation index, NDVI

$$FPAR(\mathbf{x},t) = -0.03448 + 1.379 \bullet NDVI(\mathbf{x},t) \tag{A.22}$$

where

$$NDVI = (R_{CH2} - R_{CH1})/(R_{CH2} + R_{CH1}) \tag{A.23}$$

and where R_{CH1} and R_{CH2} denote the land surface reflectances in the visible (0.58-0.68 μm) and the infrared (0.725-1.10 μm) regions of the spectrum, respectively. Previously, Heimann and Keeling [1989] expressed FPAR by a simple channel ratio, but since then NDVI has been the preferred approach by most investigators. Neither choice is based on well defined physical principles. The coefficients in equation (A.22) were set to produce a range in FPAR (**x**,t) from 0 to 1, for NDVI values ranging from 0.025 to 0.75. In those few instances where NDVI was below or above this range, FPAR was set to 0 or 1, respectively. The selected ranges are in accord with those previously selected by Heimann and Keeling [1989, p. 250].

As a source of NDVI we use a data product of the Pathfinder project [James and Kalluri, 1994] extending from July, 1981 to September, 1994. The data are composites of observations,

originally at 8 km resolution, composited to a grid spacing of 1° by 1°, and to time-intervals ranging from 8 to 11 days (days 1-10, 11-20, and the remaining days of each month). For PAR we used estimates from satellite observations of Pinker and Lazslo [1992] for the year 1986, except that for certain sensitivity tests we used data for 1987. The factor ϵ was determined by a fitting procedure described below.

To reduce the effect of residual calibration errors, the NDVI data were adjusted at each time-step by subtracting a time-variable "desert correction" consisting of a contemporary seasonally-adjusted NDVI, spatially averaged for a specified barren region. This region was defined as all grid cells from 10° to 50°N in which NDVI averaged 0.10 or less for July through August of 1981 through 1990. To affect a seasonal adjustment, interannual averages of the unadjusted desert correction were computed for each 8-11 day interval of the year, averaged from July, 1981 through June, 1991 (the period of data availability at the time the adjustment was determined). The resulting seasonal cycle was then subtracted from the unadjusted correction. The adjusted correction, on average, was 0.00977 NDVI units; its 75th percentile, 0.01363; its maximum, 0.03994.

NPP was initially calculated for each 8-11 day interval and 1° by 1° grid box of the full Pathfinder data set; it was then averaged to the 7.82° by 10.0° resolution of the TM2 transport model. Because of potential complications associated with the eruption of Mount Pinatubo in June, 1991, and the advanced age of the NOAA-11 satellite after the effects of the eruption had dissipated [Kidwell, 1995], we restricted our use of computed NPP mainly to the period before the eruption. Since we lacked NDVI data to portray interannual variability for the full period of our atmospheric CO_2 data set, we subsequently computed a spatially variable, interannually averaged seasonal cycle of NPP expressed by averages for each 8-11 day interval over calendar years 1982 through 1990. This product, similar in format to the seasonal cycle determined for the NDVI desert correction, was used for all of our inversion calculations, except certain sensitivity tests, described in Article III, which took account of the complete Pathfinder data set.

Heterotrophic respiration is specified, as described by Heimann and Keeling [1989], as a function of daily surface air temperature, $T(\mathbf{x},t)$, in which a fraction, ν_{RES}, of the flux component, $F_{RES}(\mathbf{x},t)$ is assumed to increase exponentially with temperature in proportion to the function

$$\Phi(\mathbf{x},t) = \frac{\phi(T(\mathbf{x},t))}{\int_{t-1/2}^{t+1/2} \phi(T(\mathbf{x},t'))dt'} \tag{A.24}$$

where the unit of time, t, is in years and

$$\phi(T(\mathbf{x},t)) = \begin{cases} {Q_{10}}^{(T(\mathbf{x},t)/10)} & \text{if } T(\mathbf{x},t) > -10°C \\ 0 & \text{if } T(\mathbf{x},t) \le -10°C \end{cases} \quad [4.11] \tag{A.25}$$

The remaining fraction, $1-\nu_{RES}$, is assumed to be time-invariant. The magnitude of ν_{RES} was established by an optimal fit of the composite model solution, $C_{CMPS}(\mathbf{x},t)$, to the atmospheric data at 3 stations with pronounced seasonal cycles, as noted below.

This fit could be carried out with separate model runs for F_{NPP} and F_{RES}, because the expression for $F_{RES}(\mathbf{x},t)$ is linearized by assuming it to be the sum of a term proportional to $\Phi(\mathbf{x},t)$ and a constant term depending only on the annual average, $\overline{F}_{RES}(\mathbf{x},t)$, i.e.

$$\begin{aligned} F_{RES}(\mathbf{x},t) = \nu_{RES}\Phi(\mathbf{x},t)\overline{F}_{RES}(\mathbf{x}) + \\ (1-\nu_{RES})\overline{F}_{RES}(\mathbf{x}) \end{aligned} \tag{A.26}$$

Daily average air temperatures for 1986, from Global Telecommunications System (GTS) station data [Miskus et al., 1988], were interpolated on a 1° by 1° grid for the years 1982 to 1998 by procedures described by Piper and Stewart [1996]. We computed $F_{RES}(\mathbf{x},t)$ on the same 1° by 1° grid and then composited it to the grid of the TM2 atmospheric transport model. We set Q_{10} equal to 1.5 for convenience in comparison with previous work of Keeling et al. [1989b], although a somewhat lower value would have been slightly more appropriate.

The light efficiency factor, e, and the fraction, ν_{RES}, were adjusted simultaneously to produce a best fit to seasonal CO_2 observations of 1986 represented by four harmonics at three stations in the northern hemisphere, where the influence of oceanic fluxes on the seasonality is small compared to that of the terrestrial fluxes. Stations used in the fit were Point Barrow, Alaska; La Jolla, California; and Cape Kumukahi, Hawaii. We performed a fit using atmospheric CO_2 and wind data for 1986, yielding e of 0.646 gC/MJ PAR, and ν_{RES} of 0.723. Both factors are held constant in time and space, neglecting variations that occur between different biomes and latitudes within each zone [e.g., Ruimy et al., 1994]. The error introduced by this assumption is lessened, however, by our selecting adjustable zones (see subsection A.13, below)] with more or less characteristic climatic regimes so that biases between zones tend to be compensated for by the components being adjustable.

The isotopic increment associated with F_{NPP} is prescribed by

$$\Delta\delta_{NPP}(\mathbf{x},t) = (\overline{\delta}_{PHO}(t) - \overline{\delta}_o(t))\frac{C_{NPP}(\mathbf{x},t)}{C_{CMPS}(\mathbf{x},t)} \quad [5.22] \tag{A.27}$$

and associated with F_{RES} by

$$(\Delta\delta_{RES}(\mathbf{x},t) = (\overline{\delta}_{RES}(t) - \overline{\delta}_o(t))\frac{C_{RES}(\mathbf{x},t)}{C_{CMPS}(\mathbf{x},t)} \quad [5.24] \tag{A.28}$$

where

$$\overline{\delta}_{PHO}(t) = \alpha_{ab}(1+\overline{\delta}_a(t)) - 1 \quad [5.20] \tag{A.29}$$

$$\overline{\delta}_{BIO}(t) = \alpha_{ba}(1+\overline{\delta}_b(t)) - 1 \quad [5.21] \tag{A.30}$$

$$\overline{\delta}_{RES}(t) = (1-\mu)\overline{\delta}_{PHO}(t) + \mu\overline{\delta}_{BIO}(t) \quad [5.23] \tag{A.31}$$

In equation (A.31), the term μ denotes the fraction of the global carbon pool that is long-lived, as described by Keeling et al. [1989a, Table 8, p. 189]. For μ we adopted the value of 0.4397 used previously by Heimann and Keeling [1989, after equation (5.23), p. 263]). Owing to the ^{13}C Suess effect, $\delta_{PHO}(t)$ is more negative than $\delta_{RES}(t)$.

A.11 Biospheric fertilization: Source Component $F_{FER}(t)$

In our analysis of the mass balance of the global carbon cycle, carried out from 1740 to present by single deconvolution, as described in Article I, subsection 4.2, a global sink for CO_2, F_{fer}, is computed which represents a seasonally adjusted stimulation of plant growth owing to increasing levels of atmospheric CO_2, and possibly to other causes, as described in Article I. To derive a corresponding source component, $F_{FER}(\mathbf{x},t)$, but taking account of seasonal variability in plant growth, we assume that F_{fer}, at each time step, is distributed globally and seasonally in proportion to the distribution of annual NPP averaged from 1982 to 1990, while its global integral is equal to the magnitude predicted by deconvolution in a manner consistent with a growth factor, β = 0.40 (indicating that the increase in uptake by the long-lived biosphere, per unit mass, is 40% of the fractional increase in atmospheric CO_2 concentration.) Therefore, the global integral, but not the geographic distribution of F_{FER}, varies from year to year. Seasonality is prescribed to be the same as for $F_{NPP}(\mathbf{x},t)$, prorated for each grid box to respective annual values.

Recent studies suggest that other sinks exist in northern mid- to high-latitudes, not distributed globally in proportion to NPP, e.g. a nitrogen fertilization sink (Townsend et al., 1996; Holland et al., 1997; but see Nadelhoffer et al., 1999 for a contrary view) and an afforestation sink (Houghton et al., 1994). Neglect of such sinks is not extremely critical to our analysis because our model employs adjustable zonal biospheric source components, described below, that tend to compensate for any such neglect.

The isotopic contribution associated with $F_{FER}(\mathbf{x},t)$ is prescribed similarly to that for $F_{NPP}(\mathbf{x},t)$ as

$$\Delta\delta_{FER}(\mathbf{x},t) = (\overline{\delta}_{PHO}(t) - \overline{\delta}_o(t))\frac{C_{FER}(\mathbf{x},t)}{\overline{C}_{CMPS}(\mathbf{x},t)} \quad [5.26] \tag{A.32}$$

A.12 Biospheric destruction: Source Component $\overline{F}_{DES}(\mathbf{x})$

A component, $\overline{F}_{DES}(\mathbf{x})$, representing annually averaged anthropogenic deforestation and other destructive effects on the terrestrial biosphere, was established on the basis of regional estimates of releases of biospheric CO_2 resulting from land use changes and deforestation. Following procedures described by Heimann and Keeling [1989, Appendix E], this source component is distributed in proportion to gridded NPP data within 12 regions for each of which Houghton et al., [1987, Table 1] lists net fluxes for the late 1970's with a global total of 1.791 PgC yr^{-1}. The original boundaries of the 12 regions were altered by Heimann and Keeling [1989, Figure E.1] to conform to boundaries of the 8° by 10° grid cells of the TM2 transport model. We adopted these boundaries, but replaced the formerly used NPP data with data time-averaged from 1982-1990, as described in subsection A.10, above. A global total of 2.000 PgC yr^{-1}, was adopted, as quoted by Houghton [1999] for 1980-1989. Both its values and its rate of change are uncertain [Schimel, 1995; Fernside, 1993]. We disregard its time variation in this study.

The isotopic increment associated with $\overline{F}_{DES}(\mathbf{x})$ is prescribed, similar to that for $F_{RES}(\mathbf{x},t)$, by the interannually varying expression

$$\overline{\Delta\delta}_{DES}(\mathbf{x},t) = (\overline{\delta}_{RES}(t) - \overline{\delta}_o(t))\frac{\overline{C}_{DES}(\mathbf{x})}{\overline{C}_{CMPS}(\mathbf{x})} \quad [5.25] \tag{A.33}$$

A.13 Adjustable Zonal Biospheric Source Components: $F_{BIO1}(\mathbf{x},t)$, $F_{BIO2}(\mathbf{x},t)$, $F_{BIO3}(\mathbf{x},t)$, and $F_{BIO4}(\mathbf{x},t)$

Four adjustable zonal source components simulate short-term interannual variations in biospheric fluxes. The zones pertain to the far northern latitudes (47-90°N), northern mid-latitudes (23.5-47°N), tropical (23.5°S-23.5°N), and southern mid-latitudes (23.5-55°S). Each component is distributed in proportion to annual NPP (averaged from 1982-1990), and has the same seasonality as the source component, F_{NPP}, prorated in each grid box to the ratio of its annual NPP to that of F_{NPP} (see section A.10, above). By distributing the 4 flux components in proportion to total annual NPP, account is taken of the absence of terrestrial CO_2 fluxes over barren areas, lakes, and oceanic areas within each zone.

The isotopic contributions associated with these adjustable components is assigned to be

$$\Delta\delta_{BIO_i}(\mathbf{x},t) = ((\overline{\delta}_{PHO}(t) + \overline{\delta}_{RES}(t))/2. - \overline{\delta}_o(t))\frac{\overline{C}_{BIO_i}(\mathbf{x},t)}{\overline{C}_{CMPS}(\mathbf{x},t)} \tag{A.34}$$

where C_{BIO_i} denotes the transport model response to zonal CO_2 source i $(i = 1-4)$ and other terms have the same meanings as described above. In preliminary calculations, we found that if we used $\overline{\delta}_{PHO}$ or $\overline{\delta}_{RES}$ instead of their average in equation (A.34), inferred fluxes were not different by more than 0.03 PgC yr^{-1}.

A.14 Biospheric ^{13}C Suess Effect

Analogous to the isotopic disequilibrium between oceanic carbon and atmospheric CO_2 caused by fossil fuel emissions (see section A.8), terrestrial biospheric carbon is also out of isotopic equilibrium with atmospheric CO_2. We do not consider this biospheric Suess effect, however, because it is accounted for implicitly in our specification of the isotopic ratio of the biospheric carbon pool, $\overline{\delta}_b$(t), which influences the isotopic increments for respiration and biospheric destruction via equations (A.30), (A.31) and (A.33), above. The ratio, $\overline{\delta}_b$(t), as noted in subsection A.1, above, takes full account of the global average biospheric Suess effect, calculated by the biospheric submodel of the single deconvolution procedure. There is no exclusively isotopic source component, similar to ${}^*F_{OSU}(\mathbf{x},t)$, because all of the biospheric CO_2 exchange with the atmosphere is by mass exchange involving the sum ^{13}C+^{12}C, unlike the oceanic Suess effect where ^{13}C and ^{12}C exchange at the sea surface even in the absence of a net mass exchange.

APPENDIX B
FITTING PROCEDURE

B.1 Quasi-stationary case

To establish sources and sinks of atmospheric CO_2, we adapted the general equations (A.3) and (A.6) of Appendix

A that relate a set of source components to the observed concentration and $^{13}C/^{12}C$ ratio of atmospheric CO_2. Each equation contains sets of terms, $C_i(\mathbf{x},t)$ and $\Delta\delta_i(\mathbf{x},t)$, denoting, respectively, incremental changes in concentration and $^{13}C/^{12}C$ ratio (expressed by $\delta^{13}C$ as defined by equation A.4) predicted for each source component. The following discussion refers to computations for a single year. Multiple years are independently computed.

The incremental changes, $C_i(\mathbf{x},t)$ and $\Delta\delta_i(\mathbf{x},t)$, are first individually evaluated for the locations of the observing stations, by means of the transport model, TM2, as described in the main text, section 3. Their sums then yield predictions of concentration and $\delta^{13}C$ at these stations.

To provide an optimal fit of the source components to the observations, several components are made adjustable, as described in Appendix A. The original equations (A.3) and (A.6) are therefore modified, as discussed below, such that the incremental change in concentration and $\delta^{13}C$ ratio, predicted for each of these adjustable components, contain a single adjustable factor, common to both concentration and $\delta^{13}C$ and for all stations. These factors are obtained by an optimal fit to the observations. This fitting procedure is carried out using annual averages of both model predictions and observations. Separate fits are made for yearly intervals centered on the beginning day and middle day of each calendar year.

For atmospheric CO_2 concentration, the composite model solution C_{CMPS} of equation (A.3) for a given observing station and year is modified to read

$$C_{obs} = C_o + \sum_{j=1}^{8} \cdot\, C_j + \sum_{k=1}^{4} \cdot\, C_{bio,k} + \sum_{l=1}^{3} \cdot\, C_{oce,l} \qquad \text{(B.1)}$$

where all quantities are annual averages or prescribed constants, and where subscript j refers to prescribed components, k to adjustable biospheric components; and l to adjustable oceanic components. The quantity, C_{obs}, which denotes the observed CO_2 concentration, replaces the annual average of $C_{CMPS}(\mathbf{x},t)$ of equation (A.3). The objective of the fitting procedure is to make adjustments until C_{CMPS} agrees as closely as possible with C_{obs}. (In this appendix we have omitted use of a bar to denote annual averages and the argument t, both used in Appendix A, above). As in equation (A.3), C_o denotes a background concentration of CO_2, formerly denoted $\overline{C}_o$. The sum, $\sum_{i=1}^{n} C_i(\mathbf{x},t)$, of equation (A.3) is replaced by separate sums for the model solutions with respect to prescribed and adjustable source components. The sum of adjustable components is further divided into biospheric and oceanic sums, as indicated by subscripts, *bio* and *oce*, respectively. The prescribed source components include IND, NPP, RES, DES, FER, TDE, ATL, and EXC, as described in Appendix A.

Similarly with respect to the $\delta^{13}C$ of atmospheric CO_2

$$\delta_{obs} = \delta_o + \sum_{j=1}^{10} \cdot\, \Delta\delta_j + \sum_{k=1}^{4} \cdot\, \Delta\delta_{bio,k} + \sum_{l=1}^{3} \cdot\, \Delta\delta_{oce,l} \qquad \text{(B.2)}$$

where δ_{obs} replaces $\delta_{CMPS}(\mathbf{x},t)$ of equation (A.6), and denotes the observed $\delta^{13}C$ of atmospheric CO_2, δ_o denotes a background value of $\delta^{13}C$, and subscripted $\Delta\delta$ denotes isotopic contributions of the adjustable biospheric and oceanic source components, and the eight prescribed source components, noted above, with the addition of two more, TDF and OSU.

Next, the model solution for each adjustable component, $C_{bio,k}$, or $C_{oce,l}$, is reexpressed as the product of a model solution with a standard source-strength of 1 PgC yr^{-1}, denoted by subscript r (units of ppm/(PgC yr^{-1})) and an adjustable source-strength factor, denoted by subscript s (units of PgC yr^{-1}). Thus

$$C_{bio,k} = s_{bio,k} \cdot r_{bio,k} \qquad \text{(B.3)}$$

$$C_{oce,l} = s_{oce,l} \cdot r_{oce,l} \qquad \text{(B.4)}$$

The adjustable isotopic components are similarly reexpressed as products of the same adjustable factors, $s_{bio,k}$ and $s_{oce,c}$, and isotopic model solutions for 1 PgC yr^{-1}, denoted by subscript ρ. Thus

$$\Delta\delta_{bio,k} = s_{bio,k}\ \rho_{bio,k} \qquad \text{(B.5)}$$

$$\Delta\delta_{oce,l} = s_{oce,l}\ \rho_{oce,l} \qquad \text{(B.6)}$$

By substituting these 4 expressions appropriately in equations (B.1) or (B.2), we obtain the fitting equations

$$C_{obs} = \sum_{j=1}^{8} C_j + \sum_{k=1}^{4} s_{bio,k}\ r_{bio,k} + \sum_{k=1}^{3} s_{oce,l}\ r_{oce,l} \qquad \text{(B.7)}$$

and

$$\delta_{obs} = \delta_o + \sum_{j=1}^{10} \Delta\delta_j + \sum_{k=1}^{4} s_{bio,k}\ \rho_{bio,k} + \sum_{l=1}^{3} s_{oce}\ \rho_{oce,1} \qquad \text{(B.8)}$$

Global constraints obtained from the double deconvolution, as described in Article I, are imposed on the global sums of the biospheric and oceanic source components, $F_i(\mathbf{x},t)$, of equation (A.2). The deconvolution procedure computes five such global fluxes: two oceanic fluxes, F_{ex} and $F_{ano,oce}$, and three terrestrial biospheric fluxes: F_{fer}, F_{des}, and $F_{ano,bio}$ (see Article I, subsection 4.1). All five fluxes have corresponding source components in the inversion computations. The global fluxes F_{ex}, F_{fer}, and F_{des} are equated, respectively, to the global integrals of the annual source component fluxes $\overline{F}_{EXC}$, $\overline{F}_{FER}$ and $\overline{F}_{DES}$, thus

$$F_{ex} = \int_{t=-1/2}^{1/2} \overline{F}_{EXC}(\mathbf{x},t)dt \equiv <\overline{F}_{EXC}> \qquad \text{(B.9)}$$

with similar expressions for F_{fer} and F_{des}. The anomalous global oceanic flux, $F_{ano,oce}$, is equated to the sum of the global integrals of the adjustable oceanic source components

$$F_{ano,oce} = <\overline{F}_{OCE1}> + <\overline{F}_{OCE2}> + <\overline{F}_{OCE3}> \qquad \text{(B.10)}$$

and the anomalous global biospheric flux, $F_{ano,bio}$, is equated to the sum of the adjustable biospheric source components

$$F_{ano,bio} = <\overline{F}_{BIO1}> + <\overline{F}_{BIO2}> + <\overline{F}_{BIO3}> + <\overline{F}_{BIO4}> \qquad \text{(B.11)}$$

To apply the global constraints imposed by the double deconvolution, we substitute in equations (B.7) and (B.8) for

the source strength factor of one biospheric and one oceanic component. Arbitrarily, we have chosen to substitute for the first of each series

$$s_{bio,1} = F_{ano,bio} - s_{bio,2} - s_{bio,3} - s_{bio,4} \quad \text{(B.12)}$$

$$s_{oce,1} = F_{ano,oce} - s_{oce,2} - s_{oce,3} \quad \text{(B.13)}$$

substituting equations (B.12) and (B.13) into equation (B.7) and rearranging terms, we obtain for each station

$$C_{obs} - \sum_{j=1}^{8} C_j - F_{ano,bio} \cdot r_{bio,1} - F_{ano,oce} \cdot r_{oce,1} = C_o + \sum_{k=2}^{4} s_{bio,k} \cdot r'_{bio,k} + \sum_{l=2}^{3} s_{oce,l} \cdot r'_{oce,l} \quad \text{(B.14)}$$

where, by definition

$$r'_{bio,k} = r_{bio,k} - r_{bio,1} \quad \text{(B.15)}$$

and

$$r'_{oce,l} = r_{oce,l} - r_{oce,1} \quad \text{(B.16)}$$

Similarly for δ^{13}C

$$\delta_{obs} - \sum_{j=1}^{10} \Delta\delta_j - F_{ano,bio} \cdot \rho_{bio,1} - F_{ano,oce} \cdot \rho_{oce,1} = \delta_o + \sum_{k=2}^{4} s_{bio,k} \cdot \rho'_{bio,k} + \sum_{l=2}^{3} s_{oce,l} \cdot \rho'_{oce,l} \quad \text{(B.17)}$$

where by definition

$$\rho'_{bio,k} = \rho_{bio,k} - \rho_{bio,1} \quad \text{(B.18)}$$

and

$$\rho'_{oce,l} = \rho_{oce,l} - \rho_{oce,1} \quad \text{(B.19)}$$

The isotopic contributions of the source components are related to C_{CMPS}, the composite atmospheric CO_2 response, by the expression (cf. equation (A.5))

$$\Delta\delta_i = (\delta_i - \delta_o) \cdot C_i / C_{CMPS} \quad \text{(B.20)}$$

where i refers to j, k, or l. Similarly

$$\rho_i = (\delta_i - \delta_o) \cdot r_i / C_{CMPS} \quad \text{(B.21)}$$

where ρ_i refers to either $\rho_{bio,j}$ or $\rho_{oce,k}$. Because C_{CMPS} is a function of the source strengths obtained in the fit, and is therefore unknown at the beginning of the calculation, it is initially set equal to the background concentration, C_o, the mean annual CO_2 concentration for the South Pole. The fit is then repeated with C_{CMPS} set equal to the right-hand side of equation (B.7).

As mentioned in subsection 6.1 of the main text, the strengths of two biospheric seasonal source components, $F_{NPP}(\mathbf{x}, t)$ and $F_{RES}(\mathbf{x}, t)$, are obtained by a separate fit to seasonal CO_2 observations at three northern stations. These two components express most of the seasonality of atmospheric CO_2 in the northern hemisphere. However, other components in the main annual fit contribute non-negligible seasonal variations (Table 3). Therefore, the seasonal fit is repeated with new source strengths determined in the main annual fit to account for all seasonal variations. We found that the seasonal fit had to be repeated only once to achieve satisfactory convergence between the seasonal and main annual fits.

In our application of these fitting procedures, each term in equations (B.14) and (B.17) was weighted by the inverse of the variance of the observations at the station so that the equations contributed to the solution in proportion to the quality of the observations. The variances of the observations were calculated as described by Keeling et al. [1989a, pp. 221, 229], by squaring the standard deviation obtained from the spline fit to the observations after dividing by the number of observations in the year of interest (data listed in Article I, Tables D3 and D4). The system of linear equations was solved by Gaussian elimination.

B.2 Extended response case

Our standard calculation of model solutions with the TM2 transport model assumes quasi-stationary sources and sinks, fluxes that vary so slowly in comparison to the atmospheric mixing time of about 1 year that their effect on the distribution of atmospheric CO_2 can be simulated at each time step as though they were either invariant or repeated year after year with the same seasonal cycle. For a specific year, the atmospheric transport associated with each source component, when identically repeated 4 times, produces in the model solution a CO_2 gradient field that is almost identical at the end of the third and fourth years of simulation, and is therefore almost quasi-stationary. In this section, we describe an alternative calculation with an extended response, in which the spatial gradients in the CO_2 concentration and δ^{13}C are modeled for each year as the sum of responses to sources operating over the subject year and the 3 preceding years as well. In our implementation of this extended response case, we made use of an earlier version of the inversion model in which the source components, F_{IND}, F_{UOS}, F_{ATL}, F_{NPP} and F_{RES}, and an equatorial component F_{EQU}, no longer in use, were as described by Keeling et al. [1989b]. Also, the components F_{DES} and F_{FER} were excluded. The adjustable biospheric components were the same as described in Appendix A above, but the adjustable oceanic components were F_{ATL} and F_{EQU}, as in the computations of Keeling et al. [1989b].

Specifically, each flux component is assumed to operate for the first of four years and then is set to zero. The responses for all 4 years are taken account of, in contrast to the previously described quasi-stationary calculation in which each component, not being set to zero, is assumed to repeat for 4 years with only the final year's response taken account of.

Because we have assumed invariant patterns embodied in the factors, r_i and ρ_i, the computations can be made without additional model runs by taking account of the quasi-stationary model solutions C_i for each source component, i, for each of the 4 years of the simulation. Let us denote these 4 successive

solutions as $C_{i,-3}$, $C_{i,-2}$, $C_{i,-1}$, and $C_{i,0}$. The corresponding incremental changes from year to year are then given by the relation

$$\Delta C_{i,1-t} = C_{i,t} - C_{i,t-1} \tag{B.22}$$

where $\Delta C_{i,1-t}$ denotes the change for $t = -3, -2, -1$, or 0. Changes in r_i and ρ_i, $\Delta r_{i,1-t}$ and $\Delta \rho_{i,1-t}$, respectively, are given by similar expressions. Equation (B.14) for each specific year is therefore modified to include, in addition to the flux component from the current year, contributions from sources in the 3 most recent previous years, i.e.

$$\begin{aligned} &C_{obs,t=0} - \\ &\sum_{t=-3}^{0} \left(\sum_{j=1}^{8} C_j + F_{ano,bio,t} \cdot r_{bio,1,t} + F_{ano,oce,t} \cdot r_{oce,1,t}\right) = \\ &C_o + \sum_{t=-3}^{0} \left(\sum_{k=2}^{4} s_{bio,k,t} \cdot r'_{bio,k,t} + \sum_{l=2}^{3} s_{oce,l,t} \cdot r'_{oce,l,t}\right) \end{aligned} \tag{B.23}$$

Equation (B.17) is similarly modified

$$\begin{aligned} &\delta_{obs,t=0} - \\ &\sum_{t=-3}^{0} \left(\sum_{j=1}^{10} \Delta\delta_j + F_{ano,bio,t} \cdot \rho_{bio,1,t} + F_{ano,oce,t} \cdot \rho_{oce,1,t}\right) = \\ &\delta_o + \sum_{t=-3}^{0} \left(\sum_{k=2}^{4} s_{bio,k,t} \cdot \rho'_{bio,k,t} + \sum_{l=2}^{3} s_{oce,l,t} \cdot \rho'_{oce,l,t}\right) \end{aligned} \tag{B.24}$$

To begin the calculation, for 1983, we assumed the same annual pulse for each of the 3 preceding years. The system of equations to be solved for, 2 equations for each station per year and all years from 1983 to 1996, led to a total of 252 (= 2 x 9 x 14) equations with 6 unknowns for each of 14 years.

ACKNOWLEDGMENT

Funding for this research was provided by the U.S. National Aeronautics and Space Administration, U.S. National Science Foundation, and U.S. Department of Energy by grants NASA NAG5-3469, NSF ATM 97-11882, NSF OCE 97-25995, and DOE DE-FG03-95ER62075, and by the Office of the Director of the Scripps Institution of Oceanography.

REFERENCES

[1] Andres, R. J., G. Marland, T. Boden, and S. Bischof, Carbon dioxide emissions from fossil fuel consumption and cement manufacture, 1751-1991 and an estimate of their isotopic composition and latitudinal distribution, in *The Carbon Cycle*, edited by T. M. L. Wigley and D. S. Schimel, pp. 53-62, Cambridge University Press, Cambridge, 2000.

[2] Andres, R. J., G. Marland, I. Fung, and E. Matthews, A one degree by one degree distribution of carbon dioxide emissions from fossil-fuel consumption and cement manufacture, 1950-1990, *Global Biogeochemical Cycles 10(3)*, 419-429, 1996a.

[3] Andres, R. J., G. Marland, I. Fung, and E. Matthews, A one degree by one geographic patterns of carbon dioxide emissions from fossil-fuel burning, hydraulic cement production, and gas flaring on a one degree by one degree grid cell basis: 1950 to 1990, ORNL/CDIAC, NDP058, Carbon Dioxide Analysis Center, Oak Ridge, Tenn., 1996b.

[4] Andres, R. J., G. Marland, and S. Bischof, Global and latitudinal estimates of δ^{13}C from fossil-fuel consumption and cement manufacture, ORNL/CDIAC, DB1013, Carbon Dioxide Information and Analysis Center, Oak Ridge, Tenn., 1996c.

[5] Bengtsson, L., M. Kanamitsu, P. Kallberg, and S. Uppala, FGGE 4-dimensional data assimilation at ECMWF, *American Meteorological Society Bulletin, 63*, 29-43, 1982.

[6] Boden, T. A., G. Marland, and R. J. Andres, Estimates of global, regional, and national annual CO_2 emissions from fossil-fuel burning, hydraulic cement production, and gas flaring: 1950-1992, Rep. ORNL/CDIAC-90, NDP-030/R6, 600 pp., Oak Ridge Nat. Lab., Oak Ridge, Tenn., 1996.

[7] Bolin, B., and C. D. Keeling, Large-scale atmospheric mixing as deduced from the seasonal and meridional variations of carbon dioxide, *Journal of Geophysical Research, 68*, 3899-3920, 1963.

[8] Bousquet, P., P. Ciais, P. Monfray, Y. Balkanski, M. Ramonet, and P. Tans, Influence of two atmospheric transport models on inferring sources and sinks of atmospheric CO_2, *Tellus, 48B*, 568-582, 1996.

[9] Bousquet, P., P. Ciais, P. Peylin, M. Ramonet, and P. Monfray, Inverse modeling of annual atmospheric CO_2 sources and sinks 1. Method and control inversion, *J. Geophys. Res., 104*, 26161-26178, 1999a.

[10] Bousquet, P., P. Peylin, P. Ciais, M. Ramonet, and P. Monfray, Inverse modeling of annual atmospheric CO_2 sources and sinks 2. Sensitivity study, *J. Geophys. Res., 104*, 26179-16193, 1999b.

[11] Broecker, W. S., and T. H. Peng, Interhemispheric transport of carbon dioxide by ocean circulation, *Nature, 356*, 587-589, 1992.

[12] Cooperative Atmospheric Data Integration Project, 1997.

[13] Denning, A. S., I. Y. Fung, and D. Randall, Latitudinal gradient of atmospheric CO_2 due to seasonal exchange with land biota, *Nature, 376*, 240-243, 1995.

[14] Denning, A. S., G. J. Collatz, C. Zhang, D. A. Randall, J. A. Berry, P. J. Sellers, G. D. Colello, and D. A. Dazlich, Simulations of terrestrial carbon metabolism and atmospheric CO_2 in a general circulation model Part 1: Surface carbon fluxes, *Tellus, 48B*, 521-542, 1996a.

[15] Denning, A. S., D. A. Randall, G. J. Collatz, and P. J. Sellers, Simulations of terrestrial carbon metabolism and atmospheric CO_2 in a general circulation model Part 2: Simulated CO_2 concentrations, *Tellus, 48B*, 543-567, 1996b.

[16] Draper, N., and H. Smith, Applied Regression Analysis, 2nd ed., 709 pp., John Wiley, New York, 1981.

[17] Fearnside, P. M., Deforestation in Brazilian Amazonia – the effect of population and land tenure, *Ambio 22*, 537-545, 1993.

[18] Gibson, J.K., P. Kallberg, S. Uppala, A. Nomura, and E. Serrano, ERA description, *ECMWF Reanal. Proj. Rep. Ser., 1*, 72 pp., Eur. Cent. for Medium-Range Weather Forecasts, Reading, England, 1997.

[19] Hao, W. M., and M.-H. Liu, Spatial and temporal distribution of tropical biomass burning, *Global Biogeochemical Cycles, 8*, 495-503, 1994.

[20] Heimann, M., The global atmospheric tracer model TM2, *Deutsches Klimarechenzentrum Technical Report No. 10*, 53 pp., Hamburg, Germany, 1995.

[21] Heimann, M. Atmospheric Inversion Calculations Performed for IPCC TAR, Chapter 3 (Carbon Cycle), in preparation, 2000.

[22] Heimann, M., and C. D. Keeling, A three-dimensional model of atmospheric CO_2 transport based on observed winds: 2. Model description and simulated tracer experiments, in *Aspects of Climate Variability in the Pacific and the Western Americas, Geophysical Monograph, vol. 55*, Edited by D. H. Peterson, pp. 237-275, AGU, Washington, D.C., 1989.

[23] Heimann, M. and P. Monfray, Spatial and temporal variation of the gas exchange coefficient for CO_2: 1. Data analysis and global validation, Report No. 31, 29 pages, Max-Planck-Institut f:ur Meteorologie, Hamburg, 1989.

[24] Heimann, M., G. Esser, A. Haxeltine, J. Kaduk, D. W. Kicklighter, W. Knorr, G. H. Kohlmaier, A. D. McGuire, J. Melillo, B. Moore, R. D. Otto, I. C. Prentice, W. Sauf, A. Schloss, S. Sitch, U. Wittenberg, and G. W:urth, Evaluation of terrestrial carbon cycle models through simulations of the seasonal cycle of atmospheric CO_2 - First results of a model intercomparison study, *Global Biogeochem. Cycles, 12*, 1-24, 1998.

[25] Heimann, M. and T. Kaminski, Inverse modelling approaches to infer surface trace gas fluxes from observed atmospheric mixing ratios, In: *Approaches to scaling a trace gas fluxes in ecosystems*, edited by A. F. Bowman, Elsevier Science, pp. 277-295, 1999.

[26] Holland, E. A., B. H. Braswell, J. F. Lamarque, A. Townsend, J. Sulzman, J. F. Muller, F. Dentener, G. Brasseur, H. Levy, J. E. Penner, and G. J. Roelofs, Variations in the predicted spatial distribution of atmospheric nitrogen deposition and their impact on carbon uptake by terrestrial ecosystems, *Journal of Geophysical Research, 102*, 15849-15866, 1997.

[27] Hollingsworth, A., A. C. Lorenc, M. S. Tracton, K. Arpe, G. Cats, S. Uppala, and P. Kallberg, The response of numerical weather prediction

systems to FGGE II-B data. Part I: Analyses, *Quarterly Journal of the Royal Meteorological Society, 111*, 1-66, 1985.

[28] Houghton, R. A., The annual net flux of carbon to the atmosphere from changes in land use 1850-1990, *Tellus, 51B(2)*, 298-313, 1999.

[29] Houghton, R. A., Boone, R. D., Fruci, J. R., Hobbie, J. E., Melillo, J. M., Palm, C. A., Peterson, B. J., Shaver, G. R., and Woodwell, G. M., The flux of carbon from terrestrial ecosystems to the atmosphere in 1980 due to changes in land use: Geographic distribution of the global flux, *Tellus, 39B*, 122-139, 1987.

[30] Houghton, J. T., L. G. Meira Filho, J. Bruce, H. Lee, B. A. Callander, E. Haites, N. Harris, and K. Maskell, eds., *Climate Change 1994, Radiative Forcing of Climate Change and an Evaluation of the IPCC IS92 Emission Scenarios,* 339 pages, Cambridge University Press, Cambridge, 1994.

[31] Iacobellis, S. F., R. Frouin, H. Razafimpanilo, R. C. J. Somerville, and S. C. Piper, North African savanna fires and atmospheric carbon dioxide, *J. Geophys. Res., 99*, 8321-8334, 1994.

[32] Jain, A. K., H. S. Kheshgi, and D. J. Wuebbles, A globally aggregated reconstruction of cycles of carbon and its isotopes, *Tellus, 48B*, 583-600, 1996.

[33] James, M. E., and S. N. V. Kalluri, The Pathfinder AVHRR land data set – an improved coarse resolution data set for terrestrial monitoring, *International Journal of Remote Sensing, 15*, 3347-3363, 1994.

[34] Kaminski, T., M. Heimann, and R. Giering, A coarse grid three-dimensional global inverse model of the atmospheric transport 1. Adjoint model and Jacobian matrix, *J. Geophys. Res. Atmos., 104*, 18535-18553, 1999.

[35] Keeling, C. D., R. B. Bacastow, A. F. Carter, S. C. Piper, T. P. Whorf, M. Heimann, W. G. Mook, and H. Roeloffzen, A three-dimensional model of atmospheric CO_2 transport based on observed winds: 1. Analysis of observational data, in *Aspects of Climate Variability in the Pacific and the Western Americas, Geophysical Monograph, vol. 55*, edited by D. H. Peterson, pp. 165-236, AGU, Washington, D. C., 1989a.

[36] Keeling, C. D., S. C. Piper, and M. Heimann, A three-dimensional model of atmospheric CO_2 transport based on observed winds: 4. Mean annual gradients and interannual variations, in *Aspects of Climate Variability in the Pacific and the Western Americas, Geophysical Monograph, vol. 55*, edited by D. H. Peterson, pp. 305-363, AGU, Washington, D. C., 1989b.

[37] Keeling, C. D., T. P. Whorf, M. Wahlen, and J. van der Plicht, Interannual extremes in the rate of rise of atmospheric carbon dioxide since 1980, *Nature 375*, 666-670, 1995.

[38] Keeling, C. D., S. C. Piper, R. B. Bacastow, M. Wahlen, T. P. Whorf, M. Heimann, and H. A. Meijer, Exchanges of atmospheric CO_2 and $^{13}CO_2$ with the terrestrial biosphere and oceans from 1978 to 2000. I. Global aspects, SIO Reference Series, No. 01-06 (Revised from SIO Reference Series, No. 00-21), Scripps Institution of Oceanography, San Diego, 2001.

[39] Keeling, C. D., and S. C. Piper, Exchanges of atmospheric CO_2 and $^{13}CO_2$ with the terrestrial biosphere and oceans from 1978 to 2000. IV. Critical overview, SIO Reference Series, No. 01-09 (Revised from SIO Reference Series, No. 00-24), Scripps Institution of Oceanography, San Diego, 2001.

[40] Keeling, R. F., and T. H. Peng, Transport of heat, CO_2 and O_2 by the Atlantics thermohaline circulation, *Philosophical Transactions of the Royal Society of London Series, 348*, 133-142, 1995.

[41] Kidwell, K. B., ed., *NOAA Polar Orbiter Data User's Guide,* National Oceanic and Atmospheric Administration, National Environmental Satellite, Data, and Information Service, National Climatic Data Center, Satellite Data Services Division, U.S. Government Printing Office, Washington, D.C., 1995.

[42] Law, R. M., P. J. Rayner, A. S. Denning, D. Erickson, I. Y. Fung, M. Heimann, S. C. Piper, M. Ramonet, S. Taguchi, J. A. Taylor, C. M. Trudinger, and I. G. Watterson, Variations in modeled atmospheric transport of carbon dioxide and the consequences for CO_2 inversions, *Global Biogeochemical Cycles, 10(4)*, 783-796, 1996.

[43] Louis, J. F., A parametric model of vertical eddy fluxes in the atmosphere, *Boundary Layer Meteorology, 17*, 187-202, 1979.

[44] Masarie, K. A. and P. P. Tans, Extension and integration of atmospheric carbon dioxide data into a globally consistent measurement record, *J. Geophys. Res.-Atmos., 100*, 11593-11610, 1995.

[45] Miskus, D., J. D. Laver, and F. G. Finger, The Climate Analysis Center's interactive climate assessment data base, *Preprint Volume, Fourth International Conference on Interactive Information and Processing Systems for Meteorology, Oceanography and Hydrology, January 31-February 5, 1988, Anaheim, California*, American Meteorological Society, Boston, Mass., 217-223, 1988.

[46] Monfray, P., M. Ramonet, and D. Beardsmore, Longitudinal and vertical CO_2 gradients over the subtropical/subantarctic oceanic sink, *Tellus, 48B*, 445-456, 1996.

[47] Nadelhoffer, K. J., B. A. Emmett, P. Gundersen, O. J. Kjonaas, C. J. Koopmans, P. Schleppi, A. Tietema, and R. F. Wright, Nitrogen deposition makes a minor contribution to carbon sequestration in temperate forests, *Nature, 398*, 145-148, 1999.

[48] Pinker, R. T. and I. Laszlo, Modeling surface solar irradiance for satellite applications on a global scale, *J. Appl. Meteorol., 31*, 194-211, 1992.

[49] Piper, S. C., and E. F. Stewart, A gridded global data set of daily temperature and precipitation for terrestrial biospheric modelling, *Global Biogeochemical Cycles, 10*, 757-782, 1996.

[50] Piper, S. C., C. D. Keeling, M. Heimann, and E. F. Stewart, Exchanges of atmospheric CO_2 and $^{13}CO_2$ with the terrestrial biosphere and oceans from 1978 to 2000. II. A three-dimensional tracer inversion model to deduce regional fluxes, SIO Reference Series, No. 01-07 (Revised from SIO Reference Series, No. 00-22), Scripps Institution of Oceanography, San Diego, 2001a.

[51] Piper, S. C., C. D. Keeling, and E. F. Stewart, Exchanges of atmospheric CO_2 and $^{13}CO_2$ with the terrestrial biosphere and oceans from 1978 to 2000. III. Sensitivity tests, SIO Reference Series, No. 01-08 (Revised from SIO Reference Series, No. 00-23), Scripps Institution of Oceanography, San Diego, 2001b.

[52] Press, W. H., S. A. Teukolsky, W. T. Vetterling, and B. P. Flannery, Numerical Recipes in Fortran. The Art of Scientific Computing, 2nd ed., Cambridge University Press, New York, 1992.

[53] Rayner, P. J., I. G. Enting, and C. M. Trudinger, Optimizing the CO_2 observing network for constraining sources and sinks, *Tellus, 48B*, 433-444, 1996.

[54] Rayner, P. J., I. G. Enting, and R. Langenfelds, Reconstructing the recent carbon cycle from atmospheric CO_2, $\delta^{13}C$ and O_2/N_2 observations, *Tellus, 51B*, 213-232, 1999a.

[55] Rayner, P. J., R. M. Law, and R. Dargaville, The relationship between tropical CO_2 fluxes and the El Niño-Southern Oscillation, *Geophysical Res. Lets., 26*, 493-496, 1999b.

[56] Rotty, R. M., Estimates of seasonal variation in fossil fuel CO_2 emissions, *Tellus, 39B*, 184-202, 1987.

[57] Ruimy, A., B. Saugier, and G. Dedieu, Methodology for the estimation of terrestrial net primary production from remotely sensed data, *Journal of Geophysical Research, 99*, 5263-5283, 1994.

[58] Russell, G., and J. Lerner, A new finite-differencing scheme for the tracer transport equation, *J. Appl. Meteorol., 20*, 1483-1498, 1981.

[59] Schimel, D. S., Terrestrial ecosystems and the carbon cycle, *Global Change Biol., 1*, 77-91, 1995.

[60] Tiedtke M., A comprehensive mass flux scheme for cumulus parameterization in large-scale models, *Monthly Weather Review, 117*, 1779-1800, 1989.

[61] Townsend, A. R., B. H. Braswell, E. A. Holland, and J. E. Penner, Spatial and temporal patterns in terrestrial carbon storage due to deposition of fossil fuel nitrogen, *Ecological Applications, 6*, 806-814, 1996.

[62] Watson, A. J., P. D. Nightingale, D. J. Cooper, Modelling atmosphere ocean CO_2 transfer, *Philosophical Transactions of the Royal Society of London, Series B-Biological Sciences, 348*, 125-132, 1995.

[63] Weiss, R. F., R. A. Jahnke, and C. D. Keeling, Seasonal effects of temperature and salinity on the partial pressure of CO_2 in sea water, *Nature, 300*, 511-513, 1982.

[64] Woodruff, S. D., R. J. Slutz, R. L. Jenne, and P. M. Steurer, A Comprehensive Ocean-Atmosphere Data Set, *Bulletin of the American Meteorological Society, 68(10)*, 1239-50, 1987.